Winter-Summer Contrast in the Response of Northern Hemisphere Precipitation Extremes to Climate Change

Andrew I.L. Williams[1,1] and Paul A. O'Gorman[2,2]

[1]University of Oxford
[2]MIT

November 30, 2022

Abstract

Climate models predict a distinct seasonality to future changes in daily extreme precipitation. In particular, models project that over land in the extratropical Northern Hemisphere the summer response is substantially weaker than the winter response in percentage terms. Here we decompose the projected response into thermodynamic and dynamic contributions and show that the seasonal contrast arises due to a negative dynamical contribution in northern summer due to weakened ascent, and a positive dynamical contribution and an anomalously strong thermodynamic contribution in northern winter. The negative dynamical contribution in northern summer is shown to relate to decreases in mean near-surface relative humidity with warming which suppress convection and associated upward motion in precipitation extremes. Finally, we show that the winter-summer contrast is also evident in observed trends of daily precipitation extremes in northern midlatitudes, which provides support for the contrast found in climate-model simulations.

Summer-Winter Contrast in the Response of Precipitation Extremes to Climate Change over Northern Hemisphere Land

Andrew I. L. Williams[1] and Paul A. O'Gorman[2]

[1]Atmospheric, Oceanic and Planetary Physics, Department of Physics, University of Oxford, Oxford, UK,
[2]Department of Earth, Atmospheric and Planetary Sciences, Massachusetts Institute of Technology, Cambridge, MA, USA

Key Points:

- Over Northern Hemisphere extratropical land, the projected fractional increase of precipitation extremes is weaker in summer than winter
- The summer-winter contrast is mostly driven by weakened extreme ascent in summer, which is correlated with decreased surface relative humidity
- The summer-winter contrast is also evident in observations of historical changes in daily precipitation extremes, consistent with CMIP5 models

Corresponding author: Andrew Williams, `andrew.williams@physics.ox.ac.uk`

Abstract

Climate models project a distinct seasonality to future changes in daily extreme precipitation. In particular, models project that over land in the extratropical Northern Hemisphere the summer response is substantially weaker than the winter response in percentage terms. Here we decompose the projected response into thermodynamic and dynamic contributions and show that the seasonal contrast arises due to a negative dynamic contribution in northern summer, and a positive dynamic contribution and an anomalously strong thermodynamic contribution in northern winter. The negative dynamic contribution in northern summer is due to weakened ascent and is strongly correlated with decreases in mean near-surface relative humidity which tend to inhibit convection. Finally, we show that the summer-winter contrast is also evident in observed trends of daily precipitation extremes in northern midlatitudes, which provides support for the contrast found in climate-model simulations.

Plain Language Summary

Extreme rainfall is a highly impactful aspect of the water cycle, and it is now well-established that global warming tends to increase the severity of extreme rainfall events. However, while this increase holds robustly on global scales, there is significant uncertainty associated with understanding the response of extreme rainfall to warming in different regions of the world and in different seasons. Here we focus on understanding changes in extreme rainfall in summer and winter over Northern Hemisphere extratropical land. We find that global warming has a contrasting impact on extreme rainfall over this region depending on the season considered. In winter, there are large increases in extreme rainfall with warming relative to the climatology, whereas in summer the changes are much weaker. We use a simple, physics-based approach to decompose these changes into contributions from changes in temperature and changes in ascent. Our results show that the contrasting seasonal response over this region is mostly due to decreases in extreme ascent with warming in summer, and that the 'summer-winter' contrast is already present in observed changes of extreme rainfall since the mid-20$^{\text{th}}$ century.

1 Introduction

The impacts of extreme precipitation are felt acutely across the world with consequences ranging from floods and landslides (Kirschbaum et al., 2012) to changes in ecosystems (Knapp et al., 2008). Additionally, it is now well-understood that extreme precipitation events intensify overall on a global scale in response to global warming (Wehner et al., 2020; Kharin et al., 2013; O'Gorman, 2015). On regional scales however, the response of precipitation extremes to warming is uncertain, with some regions projected to experience changes in precipitation extremes which are much higher or lower than the global-mean intensification (Pfahl et al., 2017). Put together, this makes regional changes in extreme precipitation potentially one of the most impactful consequences of global warming. Thus, understanding historical and future changes in regional extreme precipitation important not only from a scientific perspective, but also for understanding the unequal impacts of climate change (Diffenbaugh & Burke, 2019). In addition, considering precipitation extremes in different seasons helps to clarify physical drivers and can also be important for impacts.

To understand projections of changes in precipitation extremes it is useful to decompose the changes into contributions from different physical drivers. One such approach is to use the simple, physical scaling developed by O'Gorman and Schneider (2009a) which relates the intensity of precipitation extremes, P_e, to the pressure vertical velocity (ω_e) and the vertical derivative of saturation specific humidity with respect to pressure assuming a moist adiabatic lapse rate ($\frac{\mathrm{dq_s}}{\mathrm{dp}}|_{\theta^*}$),

$$P_e \sim -\left\{ \omega_e \left. \frac{\mathrm{dq}_s}{\mathrm{dp}} \right|_{\theta^*} \right\}, \tag{1}$$

where $\{\cdot\}$ denotes a mass-weighted vertical integral over the troposphere, ω_e is evaluated on the day of the extreme event, and $\frac{\mathrm{dq}_s}{\mathrm{dp}}|_{\theta^*}$ is evaluated using the temperature T_e on the day of the extreme event. Thus, when considering a change in precipitation extremes due to global warming, δP_e, we can decompose the change into a thermodynamic contribution associated with changes in T_e and a dynamic contribution associated with changes in extreme ascent ω_e,

$$\delta P_e \;\approx\; \delta P_{\mathrm{thermodynamic}} \;+\; \delta P_{\mathrm{dynamic}}. \tag{2}$$

Pfahl et al. (2017) recently showed that Eq. 1 successfully captures the present-day and future changes of precipitation extremes in simulations from the Coupled Model Intercomparison Project Phase 5, CMIP5, (Taylor et al., 2012) and thus is a good proxy for understanding and decomposing these future changes (Fig. S1). Pfahl et al. (2017) used Eq. 1 to decompose future regional changes in annual and seasonal maximum daily precipitation (hereafter, Rx1day) in the CMIP5 simulations into thermodynamic and dynamic contributions. The thermodynamic contribution is positive and relatively spatially uniform, whereas the dynamic contribution varies strongly between regions and seasons and can either locally amplify or counteract the increases from the thermodynamic contribution.

The results of Pfahl et al. (2017) show a pronounced 'summer-winter' contrast in the response of seasonal Rx1day. The fraction of Northern Hemisphere (NH) extratropical land experiencing robust increases is relatively small in June-July-August (JJA), due to a negative dynamic contribution over land, particularly over Europe and North America. Similar results were found by Tandon et al. (2018) for the CanESM2 large ensemble. By contrast, Pfahl et al. (2017) found a strong response of precipitation extremes in the NH extratropics for December-January-February (DJF), and climate change was found to induce a shift in precipitation extremes towards the cold season in this region. Marelle et al. (2018) also found a shift towards the cold season for many regions in both CMIP5 models and regional models from the Coordinated Regional Downscaling Experiment (CORDEX). Furthermore, Marelle et al. (2018) found that the CMIP5 and CORDEX models reproduce most aspects of the seasonality of precipitation extremes in the current climate when compared to gridded observations, which increases confidence in their future projections for changes in seasonality.

High-resolution, regional models have also shown a weaker response of precipitation extremes to climate change in JJA than DJF in Europe (Wood & Ludwig, 2020). This summer-winter contrast was also found in convection-permitting simulations of the Mediterranean (Pichelli et al., 2021) and the Contiguous United States (Prein et al., 2017), which is notable since convection-permitting simulations are better able to represent short-duration precipitation extremes (Prein et al., 2015). Precipitation extremes in JJA are known to be sensitive to how convection is represented (Chan et al., 2014; Prein et al., 2015; Ban et al., 2015; Kooperman et al., 2014), and caution is needed for projections in regions and seasons with significant mesoscale convective activity, particularly for sub-daily extremes. This emphasizes the importance of seeking observational evidence and robust physical mechanisms that may support projected seasonal changes in precipitation extremes.

Here, we focus on the summer-winter contrast in the fractional response of daily precipitation extremes to climate warming in the NH in CMIP5 models and gridded observations. We begin by describing the model output and observational data and the methods of analysis (Section 2). We then show that the JJA-DJF contrast is primarily due to differences in the dynamic contribution between JJA and DJF, but that differences in the thermodynamic contribution also play a role, particularly at high latitudes (Section 3). We further show that the negative dynamic contribution in JJA is strongly correlated in terms of model scatter and spatial pattern to decreases in mean near-surface relative humidity over land, suggesting a possible mechanism through a less favorable convective environment (Section 4). Finally, we demonstrate that the summer-winter contrast is also evident in gridded observational datasets and CMIP5 simulations over the historical period (Section 5), before giving our conclusions (Section 6).

2 Methods

We analyse changes over 1950–2100 under the historical and RCP8.5 scenarios for CMIP5. All models are used that provide the required data (listed in Text S1). The scaling and decomposition based on Eq. 1 is taken from Pfahl et al. (2017), and further details can be found there, but we repeat the key points of the calculation here. We chose not to repeat their calculations with CMIP6 output because there is little improvement in the simulation of daily precipitation extremes between CMIP5 and CMIP6 (Wehner et al., 2020).

Daily surface precipitation was used to calculate the maximum daily precipitation amount (Rx1day) for JJA and DJF in each year. Daily-mean temperature and vertical pressure velocity on all available pressure levels at the location and day of each daily-maximum precipitation event (T_e and ω_e, respectively) were then used to calculate the full extreme precipitation scaling following Eq. 1 by performing a vertical integral over all tropospheric levels with ascent ($\omega_e < 0$). To calculate the thermodynamic contribution, this analysis is repeated but with ω_e replaced with its average over all years from 1950-2100.

To calculate the sensitivity to climate change, we first normalize Rx1day and the full and thermodynamic scalings by dividing by their average over the historical period (1950-2000). We then calculate the dynamic contribution as the difference between the full and thermodynamic scaling. This approach to calculating the dynamic contribution differs slightly from Pfahl et al. (2017), but yields similar results (e.g., compare our Fig. 1c with their Fig. S8d). We then regress these normalized time series against global- and annual-mean surface temperature anomalies over 1950-2000 using the Theil-Sen estimator to produce sensitivities in units of (% K^{-1}). The Theil-Sen estimator is a non-parametric estimator which operates by choosing the median of the slopes of all lines through pairs of points and is less sensitive to outliers than ordinary least-squares regression. This regression approach has been shown to provide more robust results compared to taking differences in multi-decadal means (Fischer et al., 2014). When presenting results for the seasonal contrast (JJA-DJF), the sensitivities are calculated by differencing the normalized JJA and DJF time series in each grid box, before regressing this ‘difference’ time series against global-mean surface temperature anomalies for each model. Using a normalization over a reference period can sometimes produce statistical biases for changes in precipitation extremes (Donat et al., 2016; Sippel et al., 2017), but our results remain largely unchanged when using the full 1950-2100 period for normalization (Fig. S2).

All analysis is performed on each model’s native grid, and then the sensitivities are re-gridded to a uniform 1°x1° grid before calculating multi-model statistics and zonal means. Pfahl et al. (2017) noted previously that some models produce very low seasonal Rx1day at some grid points in the subtropics, which creates anomalously large extreme precipitation sensitivities. Thus, when calculating multi-model or zonal means we exclude grid boxes from models where the average seasonal Rx1day over the historical period is less than 0.5 mm day^{-1}. Additionally, we found that the CMCC-CMS model produced unrealistically large changes in the thermodynamic contribution over Pakistan and Afghanistan, and so for this model we exclude the region from 29.5° to 32.5° latitude and 60° to 68° longitude.

We also analyse changes in seasonal Rx1day over the historical period over land in observations and compare them to the same period in the CMIP5 simulations (combining the historical and RCP8.5 simulations). We analyse the 'extended' NH summer (MJJAS) and winter (NDJFM) seasons (as opposed to JJA and DJF) to improve the signal-to-noise ratio and use data from 1950-2017, with the time-period chosen for maximum overlap with the CMIP5 data. For Rx1day observations, we focus on the HadEX3 gridded dataset (Dunn et al., 2020) which has a spatial resolution of 1.25° x 1.875°, but we also show results for the GHCNDEX observational dataset over 1952-2018 (Donat et al., 2013) which has a resolution of 2.5° x 2.5° in the supplement as a point of comparison. To calculate annual- and global-mean surface temperatures (including land and ocean) from observations, we use the NOAA Merged Land-Ocean Surface Temperature Analysis (Vose et al., 2012).

Sensitivities in % K^{-1} for the observations are calculated at each gridbox as described earlier but requiring at least 45 years of data at that grid box and normalizing by an average over all the years used. When analysing the summer-winter contrast (here, MJJAS-NDJFM) we require each grid box to have 45 years of data for both seasons in each year, and we normalize each time series separately before differencing and then performing the regression. CMIP5 data are subsampled to the observations in both space and time. To reduce the influence of unforced variability and outliers, we then aggregate the sensitivities into 5° latitude bands and calculate the median sensitivity across each latitude band. We use bootstrapping to estimate the uncertainty due to inter-annual variability and the non-uniform spatial coverage of the observations. To do this we calculate 10,000 bootstrap samples per latitude band, where each sample involves a random choice of both the years used for each grid box to calculate the regression, and a random choice of the grid boxes used to calculate the median sensitivity across the latitude band. We then calculate the median sensitivity for each bootstrap sample, and then the 90% confidence interval across samples for each latitude band. Our conclusions are largely insensitive to the size of the latitude bands and the number of bootstrap samples used, except in the tropics where larger latitude bands can obscure seasonal migrations of the ITCZ.

3 Summer-Winter contrast in CMIP5

Figure 1 shows the multi-model mean patterns of seasonal Rx1day sensitivity based on the scaling Eq. 1 and its decomposition into thermodynamic and dynamic contributions for JJA, DJF and JJA-DJF. As found in previous studies, the thermodynamic contribution is relatively uniform with robust agreement on the sign and the magnitude in both seasons. In stark contrast, the dynamic contribution exhibits strong regional and seasonal variations.

The NH extratropics show a strongly negative JJA-DJF contrast especially over land (Fig. 1g). Over this region, the DJF response (Fig. 1d) is amplified by a positive contribution from the dynamics (Fig. 1f) and a relatively strong thermodynamic contribution particularly at high latitudes (Fig. 1e). On the other hand, the response during JJA is 'muted', with much less multi-model agreement and with some regions (particularly Europe and the continental United States) exhibiting close to no change or even negative responses of extreme precipitation to warming (Fig. 1a). This weak JJA response arises predominantly due to the strongly negative dynamic contribution (Fig. 1c) which cancels out the robust, positive increase due to the thermodynamic contribution (Fig. 1b). The negative dynamic contribution in JJA is particularly strong over land and parts of the subtropical Atlantic. A land-ocean contrast in the dynamic contribution in JJA is apparent when examining anomalies from the zonal-mean (Fig. S3), which show that the negative dynamic contribution extends further poleward over NH land as compared to ocean. The combination of the very weak response in JJA and the amplified response in DJF leads to the strong JJA-DJF difference in the response, particularly over NH mid-

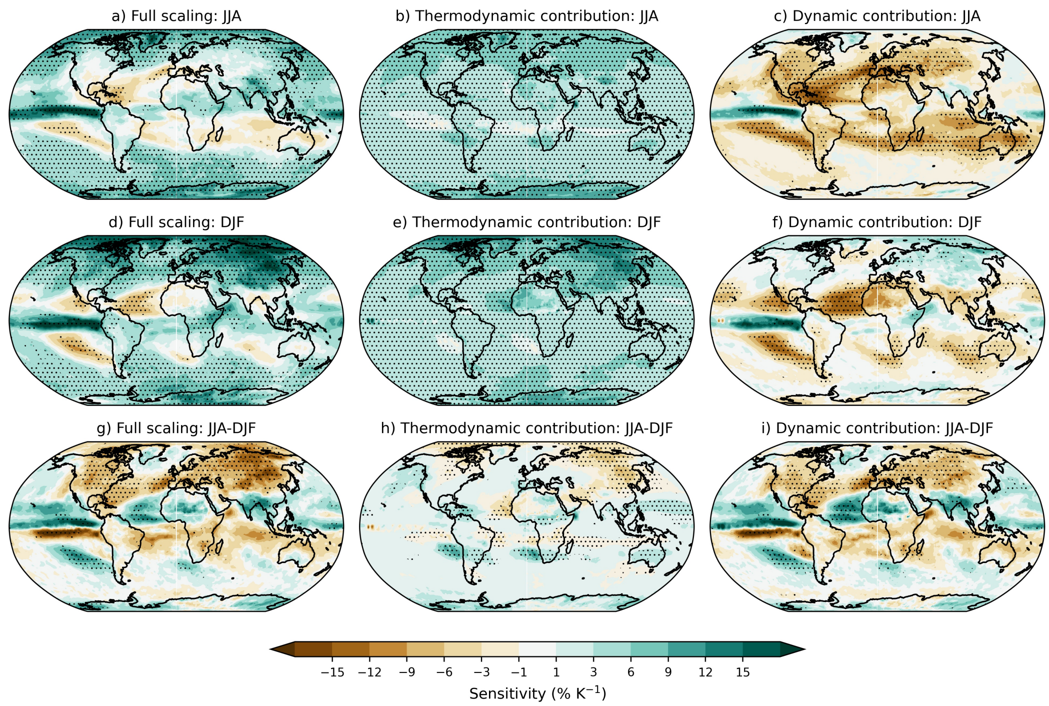

Figure 1. Multi-model mean Rx1day sensitivity over 1950-2100 according to the scaling Eq. 1 (a,d,g) and decomposition into (b,e,h) thermodynamic and (c,f,i) dynamic contributions for (a-c) JJA, (d-f) DJF and (e-i) JJA minus DJF, the summer-winter contrast. Stippling indicates where at least 90% of the models agree on the sign of the change.

latitude land. The dynamic contribution is responsible for most of the JJA-DJF difference, as illustrated by the similarity between Fig. 1g and i, but seasonal differences in the thermodynamic contribution also play a role (Fig. 1h).

We next examine zonal-mean changes in the scaling decomposition over both land and ocean and over land only (Fig. 2). The thermodynamic contribution is larger at higher latitudes (e.g., Fig. 2b,e) and is partly responsible for the JJA-DJF contrast at NH middle and high latitudes (Fig. 2c,f), implying a stronger thermodynamic contribution in DJF than JJA. A stronger thermodynamic contribution is expected for the lower temperatures in winter and at higher latitudes because percentage increases in $\frac{dq_s}{dp}|_{\theta^*}$ with increasing temperature are larger at lower temperatures (O'Gorman & Schneider, 2009a). It could also be argued that Arctic amplification of surface warming also plays a role, and indeed the JJA-DJF contrast in the NH thermodynamic contribution is negligible when we regress against zonal-mean temperature (Fig. S4). However, the stronger thermodynamic contribution at higher (and colder) latitudes is also found to occur even when a globally uniform surface warming is imposed (O'Gorman et al., 2021) suggesting that it is not tied to Arctic amplification. Additionally, previous studies have found there is less warming of T_e than mean temperature at middle and high latitudes (e.g., Fig. S5 of O'Gorman and Schneider (2009a) or Fig. 8c of O'Gorman and Schneider (2009b)) which suggests that normalizing by the local changes in zonal-mean temperature gives too much emphasis to Arctic amplification.

In the tropics, the zonal-mean results in Fig. 2 are consistent with amplification of precipitation extremes along the ITCZ region, which moves seasonally. This leads to a southward shift in precipitation extremes when considering the summer-winter con-

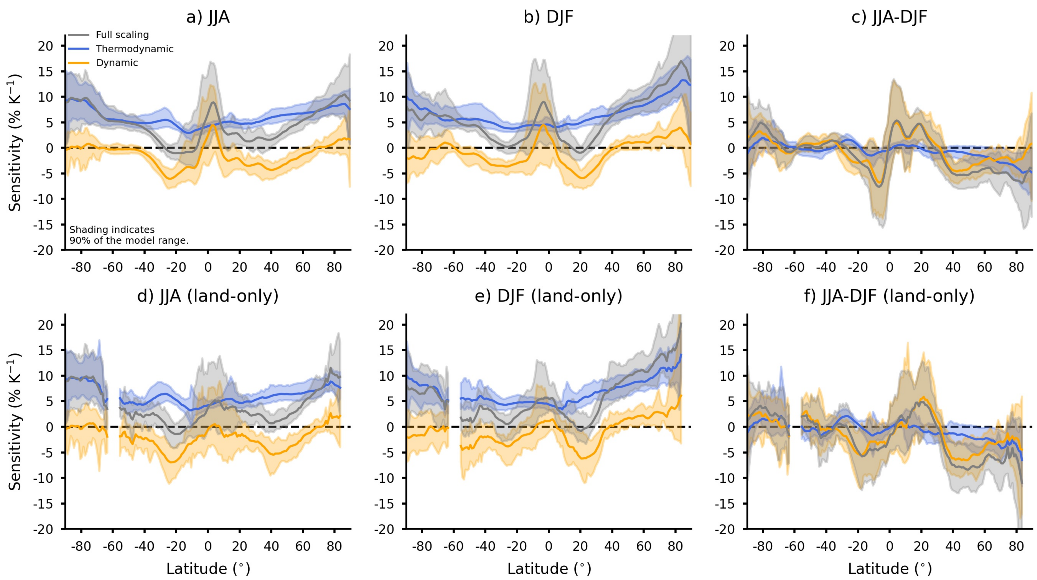

Figure 2. Zonal-mean of the Rx1day sensitivity over 1950-2100 according to the scaling and its decomposition into thermodynamic and dynamic contributions for (a) JJA, (b) DJF and (c) JJA-DJF. Lines indicate multi-model means and shading shows the 90% model range. Panels (d,e,f) show the same results but for over land only.

trast (Fig. 2c,f) because the ITCZ occurs further south in DJF than in JJA. These shifts are driven by the dynamic contribution as demonstrated by the similarity between the changes in the full scaling and the dynamic contribution in the tropics (gray and orange lines in Fig. 2c,f).

We have presented results in terms of percentage changes in (% K^{-1}) as opposed to absolute changes (mm day^{-1} K^{-1}) because it is useful to consider the change in each season relative to what is expected for that season and because previous studies have also focused on percentage changes which are easier to relate to physical processes. Absolute changes also show a seasonal contrast for much of NH midlatitude land but not for some parts of Asia (Fig. S5g) or for zonal-mean quantities (Fig. S6f), because the thermodynamic contribution offsets the dynamic contribution when considering absolute changes. Thus, one additional advantage of considering percentage changes is that it provides a strong zonal-mean signal to look for in the observational record (Section 5).

4 Physical mechanisms of the negative dynamic contribution in JJA

Dynamic weakening of precipitation extremes during JJA is a large contributor to the JJA-DJF contrast in the extratropical NH, particularly over land (Figs. 1c and 2d). Physically then, what mechanisms could be responsible for this dynamic weakening? Tandon et al. (2018) tackled this question using a three-term approximation of the QG-ω equation and found the weakening of extreme ascent was related to increases in the horizontal length scale of extreme ascent. However, Li and O'Gorman (2020) numerically inverted the QG-ω equation in extreme precipitation events and found that changes in eddy length were less important when all terms were retained in the QG-ω equation, although they did not separately analyse extremes in JJA. Changes in moist static stability, σ_m, have also been found to be important in previous studies (Li & O'Gorman, 2020; Tandon et al., 2018), with an increase in σ_m associated with a weakening of ascent. Here, we calculate changes in moist static stability on the days of the extreme events following previous work (Text S2) and find that the changes in moist static stability are mostly consistent with the spatial pattern of the JJA dynamic contribution (Fig. S7), but they fail to capture the inter-model spread in projections over NH land (Fig. S8).

We next investigate an alternative explanation for the dynamic contribution over NH extratropical land in JJA in terms of changes in the near-surface relative humidity (RH_{2m}). Decreases in RH_{2m} over land are expected with global-warming because of the land-ocean warming contrast (Byrne & O'Gorman, 2016, 2018) and decreases in stomatal conductance (Cao et al., 2010; Berg et al., 2016). Furthermore, previous work has already shown that decreases in relative humidity cause an increase in convective inhibition (CIN) that is particularly large over NH land in JJA (Chen et al., 2020).

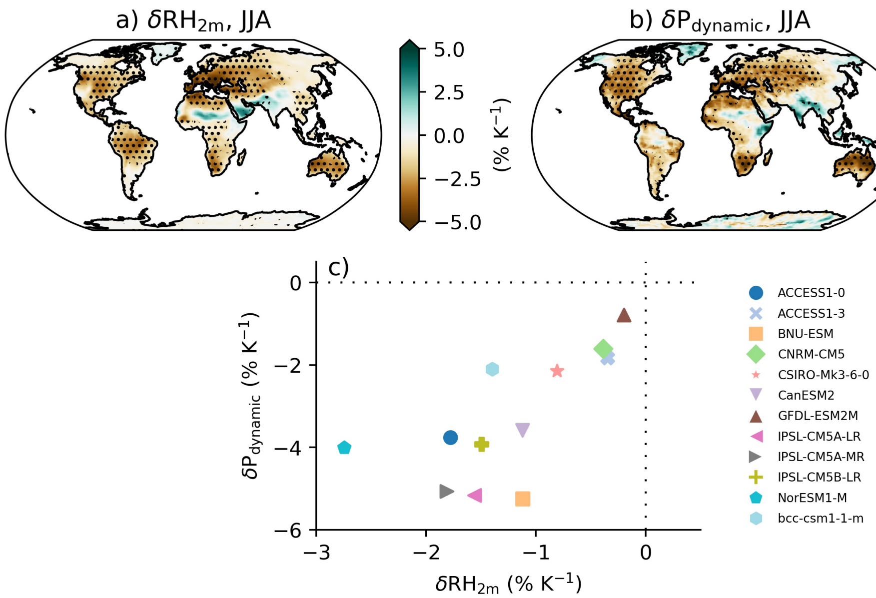

Figure 3. Sensitivity for JJA over 1950-2100 of (a) seasonal-mean near-surface relative humidity and (b) the dynamic contribution to changes in precipitation extremes. Results are shown for the 12 models that archived RH_{2m} and for which the dynamic contribution was calculated. Stippling indicates where 10 out the 12 models agree on the sign of the sensitivity. Panel (c) shows a scatter plot of the median sensitivities across land grid boxes in the latitude band 40-70°N for each model.

In Fig. 3 we compare the sensitivities of seasonal-mean RH_{2m} and the dynamic contribution to precipitation extremes during JJA for climate change over 1950-2100. The sensitivity of RH_{2m} is defined using regression analogously to the sensitivity of precipitation extremes and normalized by the 1950-2000 mean. There is strong agreement between the spatial pattern of the change in RH_{2m} and the dynamic contribution (Fig. 3a,b), with the models agreeing robustly on strong decreases in relative humidity and a negative dynamic contribution over similar regions of the globe. Furthermore, Fig. 3c shows that models with a stronger decrease in JJA RH_{2m} also tend to have a stronger negative dynamic contribution when averaged over NH midlatitude land. This suggests a mechanism whereby decreases in RH_{2m} over NH land during JJA lead to a less-favorable environment for the convective heating that amplifies ascent in precipitation extremes. The link between the dynamic contribution and RH_{2m} is not as strong in individual model runs (Fig. S9 and S10), potentially due to unforced variability in precipitation extremes and other mechanisms which act to change ω_e in precipitation extremes but are not robust across models. Changes in $\mathrm{RH_{2m}}$ on the day of the event are weaker but are nonetheless strongly correlated with the dynamic contribution (Fig. S11).

The details of the mechanism by which decreases in relative humidity inhibit convective heating in extreme precipitation events requires further study, ideally with a cloud-resolving model. One possibility is through increases in seasonal-mean CIN, which we find are correlated with the dynamic contribution for both the spatial pattern and inter-model scatter (Text S3, Fig. S12). CIN on the day of the extreme precipitation event also increases, but the correlation with the dynamic contribution is weaker (see Figs. S13-14 and discussion in Text S3). Another possibility is that decreases in relative humidity inhibit convective heating through entrainment of relatively drier environmental air, and this is plausible because the region of decreased relative humidity over land extends upwards through the lower troposphere (Chen et al., 2020).

The relationship between changes in mean relative humidity and the negative dynamic contribution to changes in extreme precipitation in JJA (Fig. 3) is notable in that it links changes in a mean quantity to changes in an extreme statistic. Such a link is potentially very useful since mean quantities can be easier to observationally constrain than extremes. The decrease in relative humidity occurs only over land, and factors such as a general weakening of the extratropical storm track in NH JJA (O'Gorman, 2010; Gertler & O'Gorman, 2019), poleward expansion of the Hadley cells in the subtropics (Pfahl et al., 2017; Norris et al., 2020), or other aspects of the large-scale dynamics (Tandon et al., 2018) may also influence the dynamic contribution over land and ocean.

In NH DJF, there is not a connection between changes in $\mathrm{RH_{2m}}$ and the dynamic contribution (Fig. S15), which we hypothesize is because daily precipitation extremes in DJF are controlled to a greater extent by large-scale dynamics as compared to the strongly convective extremes in JJA.

Interestingly, there is also a negative dynamic contribution over the Southern Hemisphere over both land and ocean in JJA (Fig. 1c). This negative dynamic contribution does not show as clear a land-ocean contrast and primarily occurs at lower latitudes as compared to the negative dynamic contribution in the NH, and thus we hypothesize it may be more strongly influenced by factors such as Hadley cell expansion (Pfahl et al., 2017; Norris et al., 2020).

5 Observed and modelled trends over the historical period

Given the difficulty in correctly representing convection in models, we next turn our attention to gridded observations of precipitation extremes. Figure 4 shows the sensitivity of daily precipitation extremes from HadEX3 observations and CMIP5 models to warming over 1950-2017 for boreal summer (MJJAS) and extended winter (NDJFM), and the seasonal contrast (MJJAS-NDJFM). The results are expressed as medians for each 5° latitude bands (see Section 2). For the NH extratropics, the observed sensitivities are positive in both MJJAS and NDJFM, and there is a clear summer-winter contrast with lower sensitivities in MJJAS than NDJFM (Fig.4a,b,c). The seasonal contrast is also evident when looking at maps of the sensitivities, but as expected there is considerable noise when considering sensitivities for a period of this length in individual grid-boxes (Fig.S16 a,b,c). The NH extratropical summer-winter contrast is also present in the CMIP5 models over the same historical period (Fig.4 d,e,f).

We next quantify the NH midlatitude response by averaging the sensitivities over land between 30-70°N with area-weighting. For the observations, the mean NH sensitivity is 5.6 % $\mathrm{K^{-1}}$ for MJJAS, 11.6 % $\mathrm{K^{-1}}$ for NDJFM, and -7.2 % $\mathrm{K^{-1}}$ for MJJAS-NDJFM. For the CMIP5 models over the same period, the multimodel-mean sensitivity and full model range are 4.4% $\mathrm{K^{-1}}$ (2.1 to 9.1 % $\mathrm{K^{-1}}$) for MJJAS, 7.0 % $\mathrm{K^{-1}}$ (4.7

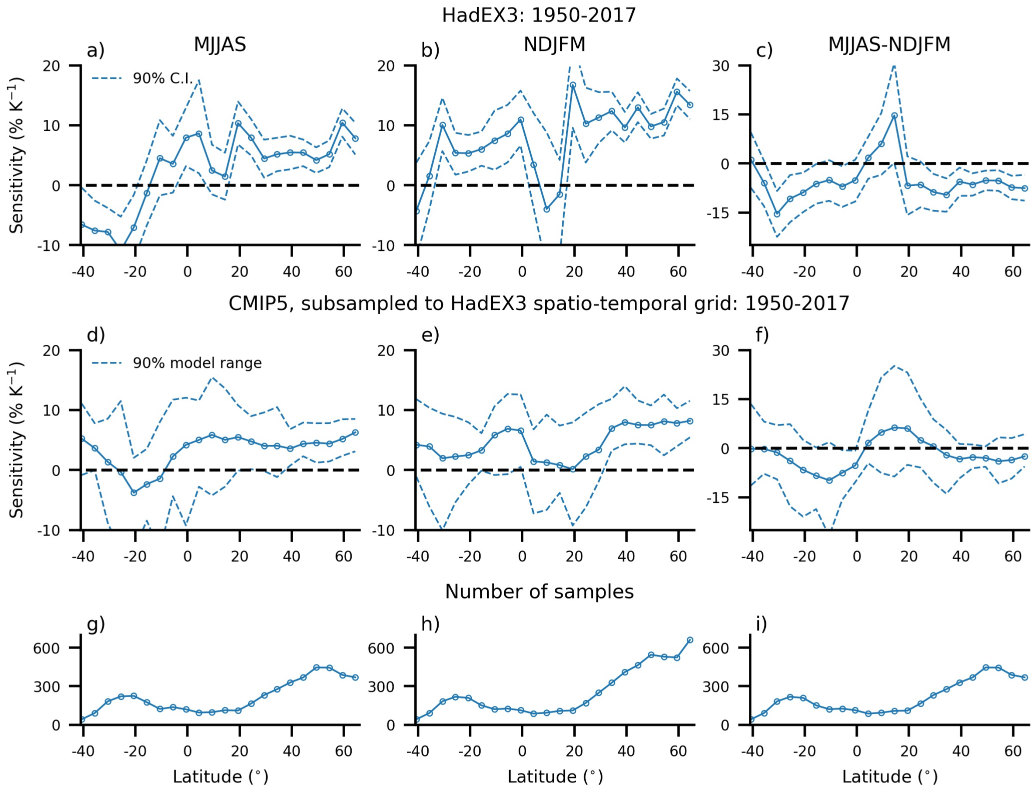

Figure 4. The sensitivity of Rx1day to warming over 1950-2017 in MJJAS (a,d), NDJFM (b,e) and MJJAS-NDJFM (c,f) for the HadEX3 dataset (a,b,c) and CMIP5 simulations subsampled to the HadEX3 dataset (d,e,f). Solid lines show the median sensitivity across the 5° latitude band. Dashed lines show the 90% confidence interval for HadEX3 and 90% of the model spread for CMIP5. The total number of samples included in each latitude band is also shown (g,h,i) which is the same for both the observations and the simulations.

to 10.8 % K^{-1}) for NDJFM, and -2.4 % K^{-1} (0.6 to -8.4 % K^{-1}) for MJJAS-NDJFM. Thus, while the models and observations show similar sensitivities during MJJAS, none of the models capture the very strong observed sensitivity for NDJFM. As a result, while the observed MJJAS-NDJFM contrast lies within the model range, the multi model-mean value is smaller in magnitude than the value in observations. The smaller magnitude of the sensitivity in the multimodel mean than in observations may be related to unforced internal variability, which is reduced by considering the multimodel mean but is likely to be still important in observations. Despite this, most but not all models (15/18) give a negative MJJAS-NDJFM contrast for this period, consistent with the observations.

GHCNDEX has a coarser spatial resolution and fewer grid boxes with data compared to HadEX3, particularly in the tropics, but we find similar changes in seasonal Rx1day over the Northern Hemisphere (Figs. S16 and S17), which strengthens our confidence in the results. Similar results are also found when the CMIP5 data are not subsampled to the observations (Figure S18), which suggests that missing grid points in the observations are not affecting our conclusions. The robust presence of the MJJAS-NDJFM contrast in observed trends over the historical period supports the contrast found in earlier sections.

6 Conclusions

In this study we have demonstrated that CMIP5 models project a robust summer-winter contrast in the response of precipitation extremes to warming over Northern Hemisphere midlatitude land, with considerably weaker percentage changes in JJA than DJF. We have also shown that this summer-winter contrast is evident in gridded observations over the historical period, which strengthens our confidence in the future projections. CMIP5 simulations over the historical period also show a summer-winter contrast that occurs in 15/18 models, and the model range includes the observed value of this contrast.

Furthermore, we have used a simple, physical scaling to help explain the cause of the summer-winter contrast in changes in precipitation extremes. The contrast is primarily caused by the dynamic contribution (related to changes in extreme ascent) with strongly negative dynamic contribution in JJA and a weakly positive dynamic contribution in DJF. The negative dynamic contribution in JJA is strong over NH extratropical land, and we show it is highly correlated with decreases in near-surface relative humidity and increases in convective inhibition in terms of spatial pattern and inter-model scatter, suggesting a potential mechanism whereby reduced relative humidity during JJA provides a less favorable environment for strong convective heating and ascent.

The thermodynamic contribution to changes in precipitation extremes also helps to amplify the response in winter over summer, particularly over high latitudes. We have focused on percentage seasonal changes because they may be more relevant for impacts in a given season and to better connect with physical mechanisms. If absolute rather than percentage changes in precipitation extremes are considered, the thermodynamic contribution is larger in summer than winter, and this offsets the JJA-DJF contrast in the dynamic contribution, although the contrast is still evident over much of NH midlatitude land (Fig. S5).

Future work could build on our observational analysis by performing a formal detection and attribution analysis of the seasonal difference in trends of precipitation extremes. Future work could also build more understanding of the positive dynamic contribution in the NH extratropics in winter, which is important as DJF is the season of maximum daily precipitation in many regions (Marelle et al., 2018). Future work could also investigate the detailed mechanism (e.g., involving CIN or convective entrainment) and physical accuracy of the link between changes in relative humidity and precipitation extremes in summer using idealized experiments in cloud-resolving models. Given the potential importance of decreases in relative humidity over land for convection and precipitation extremes, it would be helpful to develop an emergent constraint for the magnitude of the expected decrease, although this may be difficult to the extent that it depends both on the land-ocean warming contrast and the plant physiological response to increased on CO_2 levels.

7 Open Research

Processed observational and climate model data supporting the conclusions in this study can be found at https://doi.org/10.5281/zenodo.6341493.

Acknowledgments

A.I.L.W. acknowledges funding from the Natural Environment Research Council, Oxford DTP, award NE/S007474/1 and the Laidlaw Research and Leadership Programme. P.A.O'.G. acknowledges support from NSF awards AGS-1552195 and AGS-1749986.

We acknowledge the World Climate Research Programme's Working Group on Coupled Modelling, which is responsible for CMIP, and we thank the climate modeling groups for producing and making available their model output. We thank Stephan Pfahl for generously providing the CMIP5 scaling data used for this study and Ziwei Li for helpful discussions. A.I.L.W. thanks Makayla Haussler for moral support and input on the figures.

References

Ban, N., Schmidli, J., & Schär, C. (2015). Heavy precipitation in a changing climate: Does short-term summer precipitation increase faster? *Geophysical Research Letters*, *42*(4), 1165–1172. doi: 10.1002/2014GL062588

Berg, A., Findell, K., Lintner, B., Giannini, A., Seneviratne, S. I., van den Hurk, B., ... Milly, P. C. D. (2016). Land–atmosphere feedbacks amplify aridity increase over land under global warming. *Nature Climate Change*, *6*(9), 869–874. doi: 10.1038/nclimate3029

Byrne, M. P., & O'Gorman, P. A. (2016). Understanding decreases in land relative humidity with global warming: Conceptual model and GCM simulations. *Journal of Climate*, *29*(24), 9045–9061. doi: 10.1175/JCLI-D-16-0351.1

Byrne, M. P., & O'Gorman, P. A. (2018). Trends in continental temperature and humidity directly linked to ocean warming. *Proceedings of the National Academy of Sciences*, *115*(19), 4863–4868. doi: 10.1073/pnas.1722312115

Cao, L., Bala, G., Caldeira, K., Nemani, R., & Ban-Weiss, G. (2010). Importance of carbon dioxide physiological forcing to future climate change. *Proceedings of the National Academy of Sciences*, *107*(21), 9513–9518. doi: 10.1073/pnas.0913000107

Chan, S. C., Kendon, E. J., Fowler, H. J., Blenkinsop, S., Roberts, N. M., & Ferro, C. A. T. (2014). The value of high-resolution met office regional climate models in the simulation of multihourly precipitation extremes. *Journal of Climate*, *27*(16), 6155–6174. doi: 10.1175/JCLI-D-13-00723.1

Chen, J., Dai, A., Zhang, Y., & Rasmussen, K. L. (2020). Changes in convective available potential energy and convective inhibition under global warming. *Journal of Climate*, *33*(6), 2025–2050. doi: 10.1175/JCLI-D-19-0461.1

Diffenbaugh, N. S., & Burke, M. (2019). Global warming has increased global economic inequality. *Proceedings of the National Academy of Sciences*, *116*(20), 9808–9813. doi: 10.1073/pnas.1816020116

Donat, M. G., Alexander, L. V., Yang, H., Durre, I., Vose, R., Dunn, R. J. H., ... Kitching, S. (2013). Updated analyses of temperature and precipitation extreme indices since the beginning of the twentieth century: The HadEX2 dataset. *Journal of Geophysical Research: Atmospheres*, *118*(5), 2098–2118. doi: 10.1002/jgrd.50150

Donat, M. G., Lowry, A. L., Alexander, L. V., O'Gorman, P. A., & Maher, N. (2016). More extreme precipitation in the world's dry and wet regions. *Nature Climate Change*, *6*(5), 508–513. doi: 10.1038/nclimate2941

Dunn, R. J. H., Alexander, L. V., Donat, M. G., Zhang, X., Bador, M., Herold, N., ... Bin Hj Yussof, M. N. (2020). Development of an updated global land in situ-based data set of temperature and precipitation extremes: HadEX3. *Journal of Geophysical Research: Atmospheres*, *125*(16), e2019JD032263. doi: 10.1029/2019JD032263

Fischer, E. M., Sedláček, J., Hawkins, E., & Knutti, R. (2014). Models agree on forced response pattern of precipitation and temperature extremes. *Geophysical Research Letters*, *41*(23), 8554–8562. doi: 10.1002/2014GL062018

Gertler, C. G., & O'Gorman, P. A. (2019). Changing available energy for extratropical cyclones and associated convection in northern hemisphere summer. *Proceedings of the National Academy of Sciences*, *116*(10), 4105–4110. doi: 10.1073/pnas.1812312116

Kharin, V. V., Zwiers, F. W., Zhang, X., & Wehner, M. (2013). Changes in temperature and precipitation extremes in the CMIP5 ensemble. *Climatic Change*, *119*(2), 345–357. doi: 10.1007/s10584-013-0705-8

Kirschbaum, D., Adler, R., Adler, D., Peters-Lidard, C., & Huffman, G. (2012). Global distribution of extreme precipitation and high-impact landslides in 2010 relative to previous years. *Journal of Hydrometeorology*, *13*(5), 1536–1551. doi: 10.1175/JHM-D-12-02.1

Knapp, A. K., Beier, C., Briske, D. D., Classen, A. T., Luo, Y., Reichstein, M., ... Weng, E. (2008). Consequences of more extreme precipitation regimes for terrestrial ecosystems. *BioScience*, *58*(9), 811–821.

Kooperman, G. J., Pritchard, M. S., & Somerville, R. C. J. (2014). The response of US summer rainfall to quadrupled CO2 climate change in conventional and superparameterized versions of the NCAR community atmosphere model. *Journal of Advances in Modeling Earth Systems*, *6*(3), 859–882. doi: 10.1002/2014MS000306

Li, Z., & O'Gorman, P. A. (2020). Response of vertical velocities in extratropical precipitation extremes to climate change. *Journal of Climate*, *33*(16), 7125–7139. doi: 10.1175/JCLI-D-19-0766.1

Marelle, L., Myhre, G., Hodnebrog, , Sillmann, J., & Samset, B. H. (2018). The changing seasonality of extreme daily precipitation. *Geophysical Research Letters*, *45*(20), 11,352–11,360. doi: 10.1029/2018GL079567

Norris, J., Chen, G., & Li, C. (2020). Dynamic amplification of subtropical extreme precipitation in a warming climate. *Geophysical Research Letters*, *47*(14), e2020GL087200. doi: https://doi.org/10.1029/2020GL087200

O'Gorman, P. A., & Schneider, T. (2009a). The physical basis for increases in precipitation extremes in simulations of 21st-century climate change. *Proceedings of the National Academy of Sciences*, *106*(35), 14773–14777. doi: 10.1073/pnas.0907610106

O'Gorman, P. A. (2010). Understanding the varied response of the extratropical storm tracks to climate change. *Proceedings of the National Academy of Sciences*, *107*(45), 19176–19180. doi: 10.1073/pnas.1011547107

O'Gorman, P. A. (2015). Precipitation extremes under climate change. *Current Climate Change Reports*, *1*(2), 49–59. doi: 10.1007/s40641-015-0009-3

O'Gorman, P. A., Li, Z., Boos, W. R., & Yuval, J. (2021). Response of extreme precipitation to uniform surface warming in quasi-global aquaplanet simulations at high resolution. *Philosophical Transactions of the Royal Society A: Mathematical, Physical and Engineering Sciences*, *379*(2195), 20190543. doi: 10.1098/rsta.2019.0543

O'Gorman, P. A., & Schneider, T. (2009b). Scaling of precipitation extremes over a wide range of climates simulated with an idealized gcm. *Journal of Climate*, *22*(21), 5676 - 5685. doi: 10.1175/2009JCLI2701.1

Pfahl, S., O'Gorman, P. A., & Fischer, E. M. (2017). Understanding the regional pattern of projected future changes in extreme precipitation. *Nature Climate Change*, *7*(6), 423–427. doi: 10.1038/nclimate3287

Pichelli, E., Coppola, E., Sobolowski, S., Ban, N., Giorgi, F., Stocchi, P., ... Vergara-Temprado, J. (2021). The first multi-model ensemble of regional climate simulations at kilometer-scale resolution part 2: historical and future simulations of precipitation. *Climate Dynamics*, *56*(11), 3581–3602. doi: 10.1007/s00382-021-05657-4

Prein, A. F., Langhans, W., Fosser, G., Ferrone, A., Ban, N., Goergen, K., ... Leung, R. (2015). A review on regional convection-permitting climate modeling: Demonstrations, prospects, and challenges. *Reviews of Geophysics*, *53*(2), 323–361. doi: 10.1002/2014RG000475

Prein, A. F., Rasmussen, R. M., Ikeda, K., Liu, C., Clark, M. P., & Holland, G. J. (2017). The future intensification of hourly precipitation extremes. *Nature Climate Change*, *7*(1), 48–52. doi: 10.1038/nclimate3168

Sippel, S., Zscheischler, J., Heimann, M., Lange, H., Mahecha, M. D., van Oldenborgh, G. J., ... Reichstein, M. (2017). Have precipitation extremes and annual totals been increasing in the world's dry regions over the last 60 years? *Hydrology and Earth System Sciences*, *21*(1), 441–458. doi: 10.5194/hess-21-441-2017

Tandon, N. F., Nie, J., & Zhang, X. (2018). Strong influence of eddy length on boreal summertime extreme precipitation projections. *Geophysical Research Letters*, *45*(19), 10,665–10,672. doi: 10.1029/2018GL079327

Taylor, K. E., Stouffer, R. J., & Meehl, G. A. (2012). An overview of CMIP5 and the experiment design. *Bulletin of the American Meteorological Society*, *93*(4), 485–498. doi: 10.1175/BAMS-D-11-00094.1

Vose, R. S., Arndt, D., Banzon, V. F., Easterling, D. R., Gleason, B., Huang, B., ... Wuertz, D. B. (2012). NOAA's merged land–ocean surface temperature analysis. *Bulletin of the American Meteorological Society*, *93*(11), 1677–1685. doi: 10.1175/BAMS-D-11-00241.1

Wehner, M., Gleckler, P., & Lee, J. (2020). Characterization of long period return values of extreme daily temperature and precipitation in the CMIP6 models: Part 1, model evaluation. *Weather and Climate Extremes*, *30*, 100283. doi: 10.1016/j.wace.2020.100283

Wood, R. R., & Ludwig, R. (2020). Analyzing internal variability and forced response of subdaily and daily extreme precipitation over europe. *Geophysical Research Letters*, *47*(17), e2020GL089300. doi: 10.1029/2020GL089300

Supporting Information for "Summer-Winter Contrast in the Response of Precipitation Extremes to Climate Change over Northern Hemisphere Land"

Andrew I. L. Williams[1] and Paul A. O'Gorman[2]

[1]Atmospheric, Oceanic and Planetary Physics, Department of Physics, University of Oxford, Oxford, UK

[2]Department of Earth, Atmospheric and Planetary Sciences, Massachusetts Institute of Technology, Cambridge, MA, USA

Contents of this file

Text S1-S3 and Figures S1-S18.

Introduction

This document provides supporting text and figures for the main article.

1. Text S1 describes the CMIP5 models used in this study.
2. Text S2 describes the calculation of the moist stability.
3. Text S3 describes the calculation of CAPE and CIN and their changes.
4. Figures S1-S18 support the findings in the main text.

Corresponding author: A. Williams, Department of Atmospheric, Oceanic and Planetary Physics, Department of Physics, University of Oxford, Oxford, UK. (andrew.williams@physics.ox.ac.uk)

Text S1.

We use the following 18 CMIP5 models: ACCESS1-0, ACCESS1-3, BNU-ESM, CMCC-CESM, CMCC-CM, CMCC-CMS, CNRM-CM5, CSIRO-Mk3-6-0, CanESM2, FGOALS-g2, GFDL-ESM2M, IPSL-CM5A-LR, IPSL-CM5A-MR, IPSL-CM5B-LR, MPI-ESM-LR, MPI-ESM-MR, NorESM1-M, bcc-csm1-1-m.

However, Fig. 3 and S9-S15 required $\mathrm{RH_{2m}}$ ('hurs') which was only available for the following 12 CMIP5 models: ACCESS1-0, ACCESS1-3, BNU-ESM, CNRM-CM5, CSIRO-Mk3-6-0, CanESM2, GFDL-ESM2M, IPSL-CM5A-LR, IPSL-CM5A-MR, IPSL-CM5B-LR, NorESM1-M, bcc-csm1-1-m.

Text S2.

We examine the fractional changes in 500hPa moist static stability, σ_m, for the same subset of CMIP5 models used in Fig. 3, on the day of the extreme event in JJA. The moist static stability, σ_m, is defined as,

$$\sigma_m = -\frac{\mathrm{RT}}{p\theta}\left(\frac{\partial\theta}{\partial p} - \left.\frac{\partial\theta}{\partial p}\right|_{\theta^*}\right),$$

where R is the gas constant for dry air, T is the temperature, θ is the dry potential temperature and $\frac{\partial\theta}{\partial p}|_{\theta^*}$ is the vertical gradient of dry potential temperature for a moist adiabatic lapse rate (assuming constant saturated equivalent potential temperature, θ^*). All quantities are taken on the day of the extreme event in JJA, and the calculation is performed on standard pressure levels. This definition of moist static stability is similar to that used by Tandon et al. (2018) and Li and O'Gorman (2020).

The multi-model mean values of σ_m^e in the control climate (1950-2000) are presented in Fig. S7a and the sensitivities with warming are presented in Fig. S7b. Because the climatological σ_m^e changes sign from negative to positive near our area of interest (the NH midlatitudes), we present absolute rather than percentage trends. Note that in the expression for the change in vertical velocity from the QG-omega equation (Equation 12 from Li and O'Gorman (2020)), the moist static stability appears in the denominator but not on its own, so it is not a problem for it to be zero or weakly negative in the control climatology.

Text S3.

We calculate CIN and CAPE for each of the models included in Fig. 3 using the `xcape` python package (Lepore et al., 2021). CAPE is taken as the vertical integral of the positive buoyancy of a parcel lifted pseudo-adiabatically from the surface, and CIN is defined similarly but for the negative buoyancy. Freezing is treated using a mixed-phase range, with the fraction of ice decreasing linearly from one at -40°C to zero at 0°C. The calculations are performed using daily temperature and specific humidity on pressure levels and at the surface. Daily surface pressure was not available for all of the models and so we used monthly-mean surface pressure. When calculating CIN and CAPE on a given day in JJA, we use monthly surface pressure for the month that contains the day. Changes in seasonal mean CIN in JJA are shown in Fig. S12. CIN^e and CAPE^e (which are evaluated on the day of the Rx1day event) and their sensitivities to warming are presented in Fig. S13-S14.

CIN^e does increase over NH extratropical land during JJA, but the increases are weak and not well correlated with the dynamic contribution (Fig. S14). The weak correlation is likely because CIN is likely to be relatively small in the period around the extreme precipitation event in order for the event to occur. For this reason, seasonal-mean CIN may be more relevant than CIN^e, with increased seasonal-mean CIN limiting the extreme event to certain days which are not as optimal for ascent in terms of other factors such as the large-scale forcing. Further study is needed to investigate the influence of CIN and convective entrainment of lower relative-humidity environmental air on the dynamic contribution, ideally using a cloud-resolving model.

We also find increases in CAPE with warming on the day of the extreme event in JJA (Fig. S13d), which might be thought to imply a positive dynamic contribution. However, previous work has documented a negative dynamic contribution is possible despite CAPE increases (Muller et al., 2011) because CAPE increases with warming mostly reflect increased buoyancy in the upper troposphere (e.g., Singh and O'Gorman (2013)) where specific humidities are small, and thus are not necessarily as important for precipitation extremes.

References

Lepore, C., Allen, J., & Abernathey, R. (2021). *xcape.* Zenodo. doi: 10.5281/zenodo.5270332

Li, Z., & O'Gorman, P. A. (2020). Response of vertical velocities in extratropical precipitation extremes to climate change. *Journal of Climate*, *33*(16), 7125–7139. doi: 10.1175/JCLI-D-19-0766.1

Muller, C. J., O'Gorman, P. A., & Back, L. E. (2011). Intensification of precipitation extremes with warming in a cloud-resolving model. *Journal of Climate*, *24*(11), 2784 - 2800. doi: 10.1175/2011JCLI3876.1

Singh, M. S., & O'Gorman, P. A. (2013). Influence of entrainment on the thermal stratification in simulations of radiative-convective equilibrium. *Geophysical Research Letters*, *40*(16), 4398-4403. doi: https://doi.org/10.1002/grl.50796

Tandon, N. F., Nie, J., & Zhang, X. (2018). Strong influence of eddy length on boreal summertime extreme precipitation projections. *Geophysical Research Letters*, *45*(19), 10,665–10,672. doi: 10.1029/2018GL079327

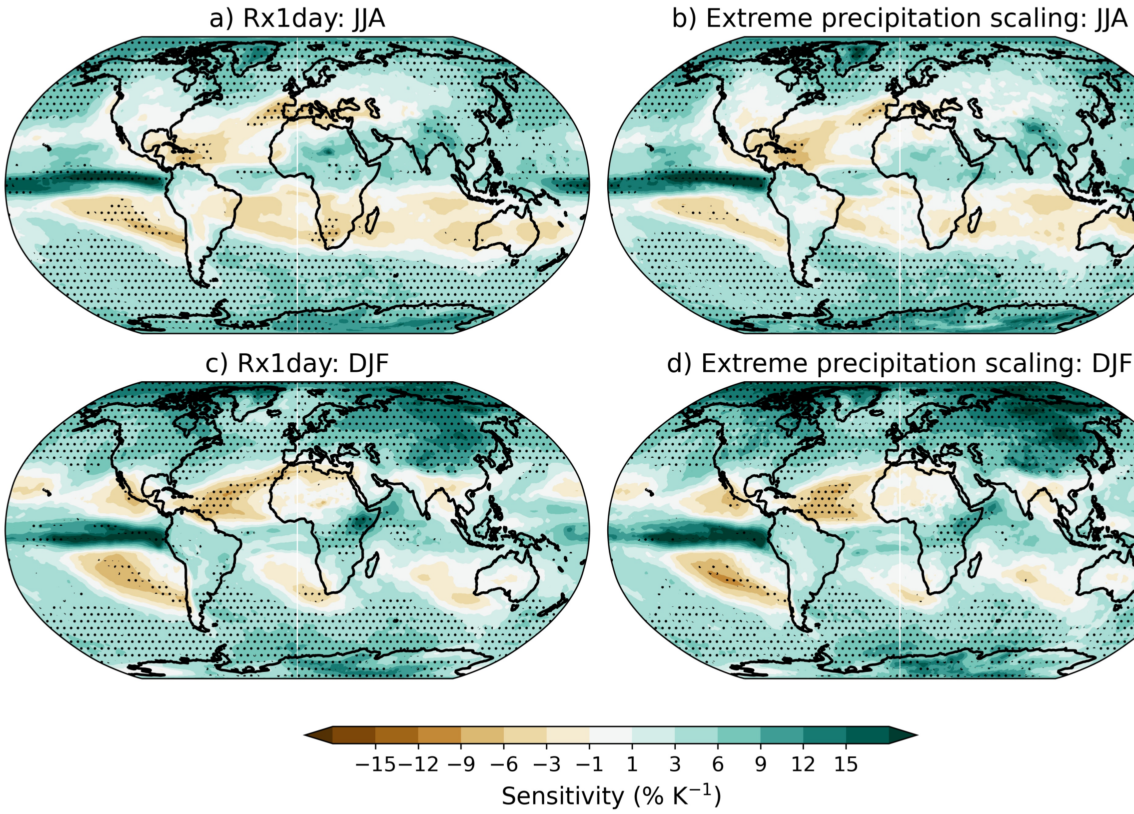

Figure S1. Comparison between CMIP5 multi-model mean changes in seasonal daily maximum precipitation (Rx1day) in JJA (a) and DJF (c) and changes in the corresponding scaling estimate calculated from Eq. 1 in the main text (b, d). Stippling indicates where at least 90% models agree on the sign of the change.

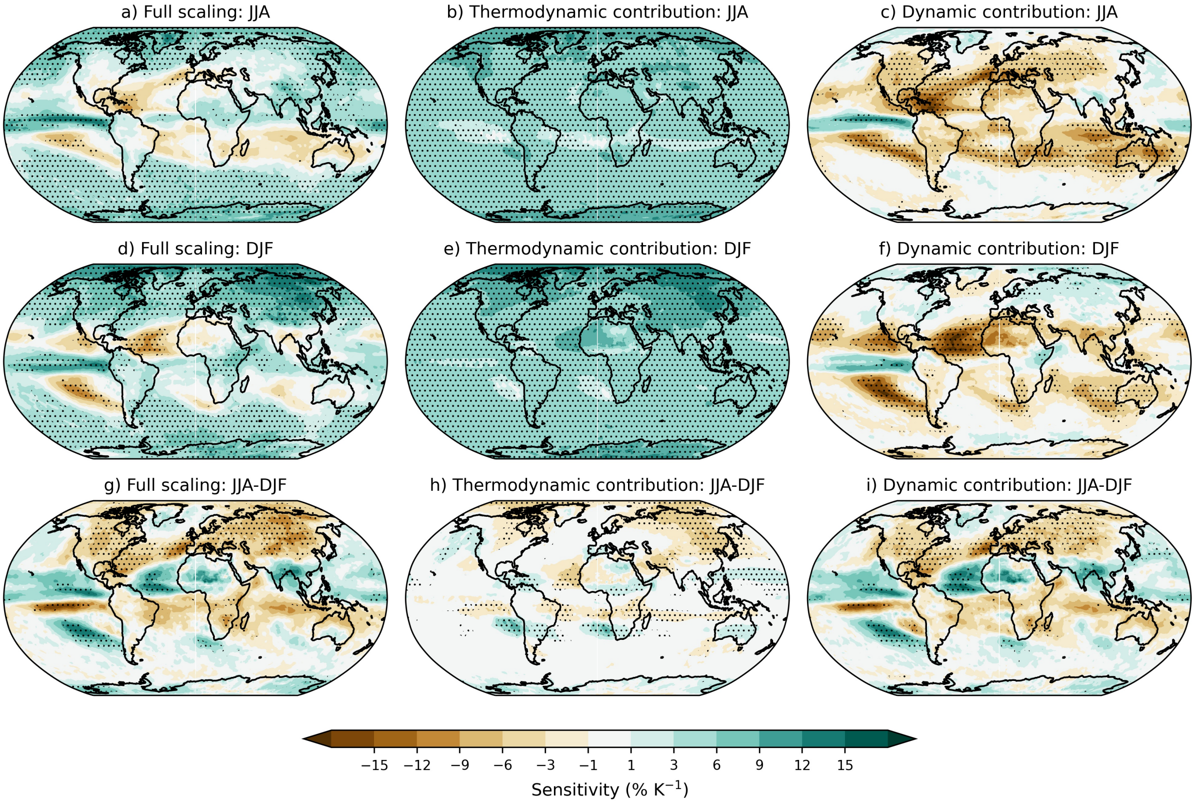

Figure S2. As in Fig. 1 except that the normalization is over the period 1950-2100 instead of 1950-2000. The results are generally similar to the results in Fig. 1.

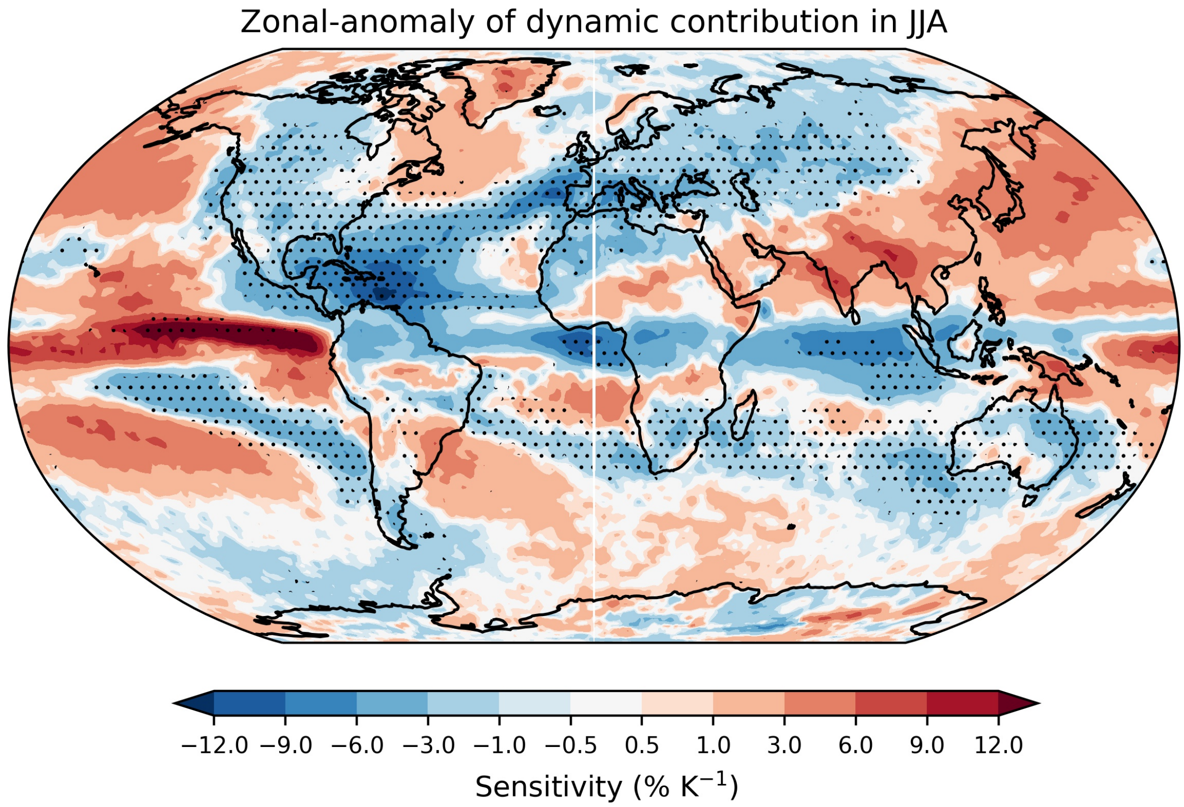

Figure S3. As in Fig. 1c except we plot the anomaly from the zonal mean.

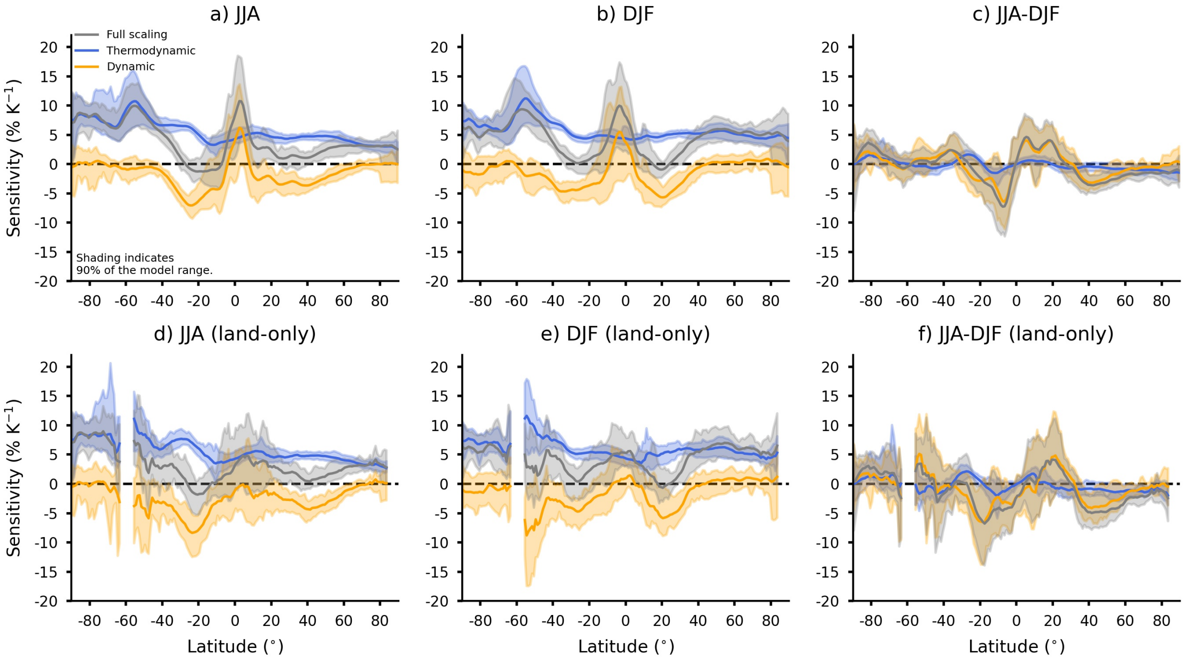

Figure S4. As in Fig. 2 except that here we show the sensitivity with respect to changes in zonal-mean temperature change rather than global-mean temperature change. There is a JJA-DJF contrast over NH extratropical land, driven by the dynamic contribution, which is robust across the CMIP5 models considered. The main difference from Fig. 2 is that the JJA-DJF contrast in the thermodynamic contribution is substantially weaker when regressing against zonal-mean temperature.

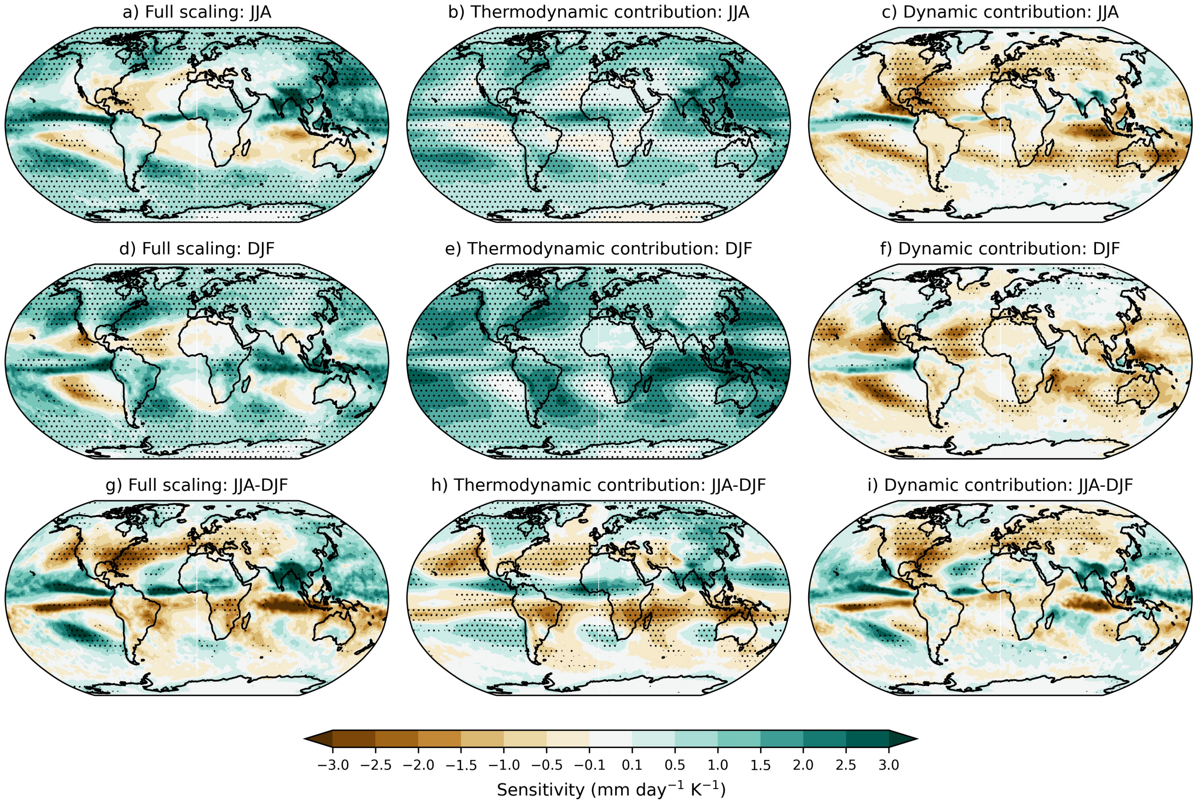

Figure S5. As in Fig. 1 except that here we do not normalize the daily maximum time-series by their average over the 1950-2000 period, and thus the trends are in mm day^{-1} K^{-1} as opposed to % K^{-1}. There is still a JJA-DJF contrast in changes in precipitation extremes over much of NH midlatitude land but not to the same extent as when percentage changes are considered.

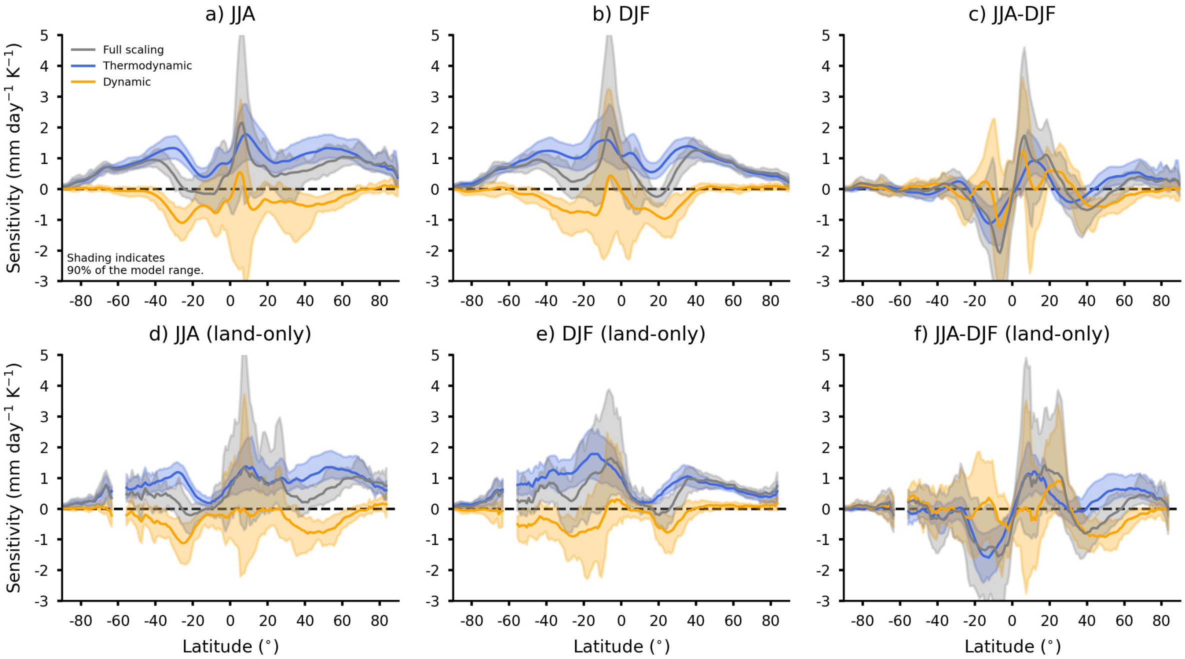

Figure S6. As in Fig. 2 except that here we do not normalize the daily maximum time-series by their average over the 1950-2000 period, and thus the trends are in mm day^{-1} K^{-1} as opposed to % K^{-1}. This figure demonstrates that while the dynamic contribution still contributes to a JJA-DJF contrast over the NH in absolute terms, it is largely cancelled out in the zonal mean at higher latitudes by weaker thermodynamic trends in DJF than in JJA.

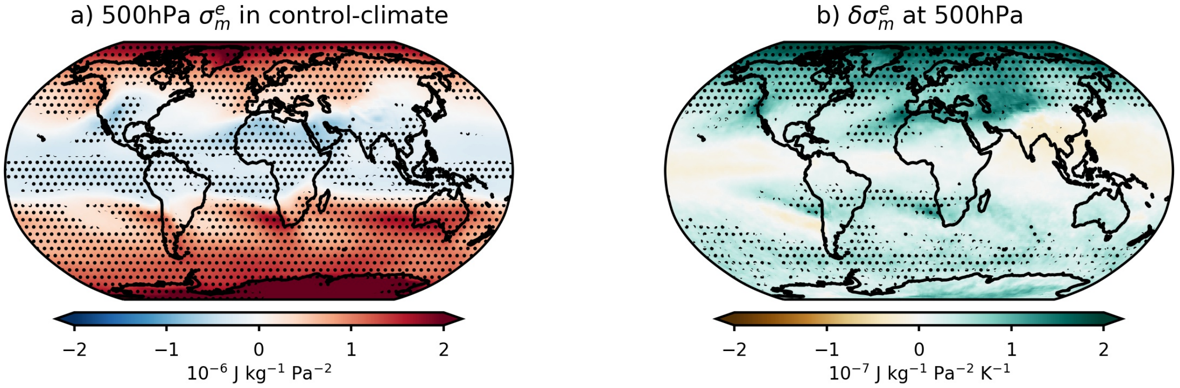

Figure S7. (a) Multi-model mean moist static stability, σ_m^e, at 500hPa calculated on the day of the extreme event in JJA and then averaged from 1950-2000. (b) Sensitivity of σ_m^e at 500hPa to global-mean warming, where absolute rather than fractional changes are used here because σ_m^e changes sign in the NH midlatitudes in the control-climate. Stippling indicates 90% model agreement.

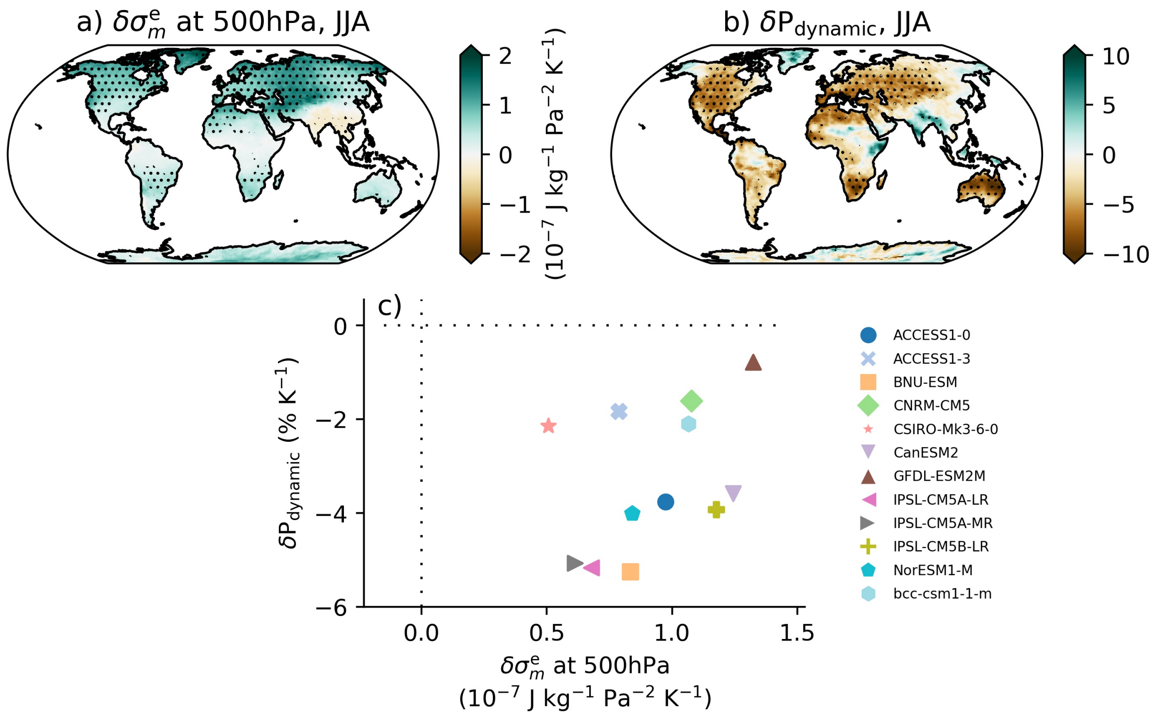

Figure S8. As in Fig. 3 except we have replaced seasonal-mean surface relative humidity with moist static stability at 500hPa on the day of the extreme event, σ_m^e. Note that absolute rather than fractional changes in σ_m^e are used to define its sensitivity to warming. The results show that σ_m^e changes correlate with the dynamic contribution in terms of spatial pattern but not inter-model scatter. (Note that in panel c there is a hint that a more negative dynamic contribution is associated with a smaller increase in moist static stability, but this is the opposite of what would be expected from a physical point of view.)

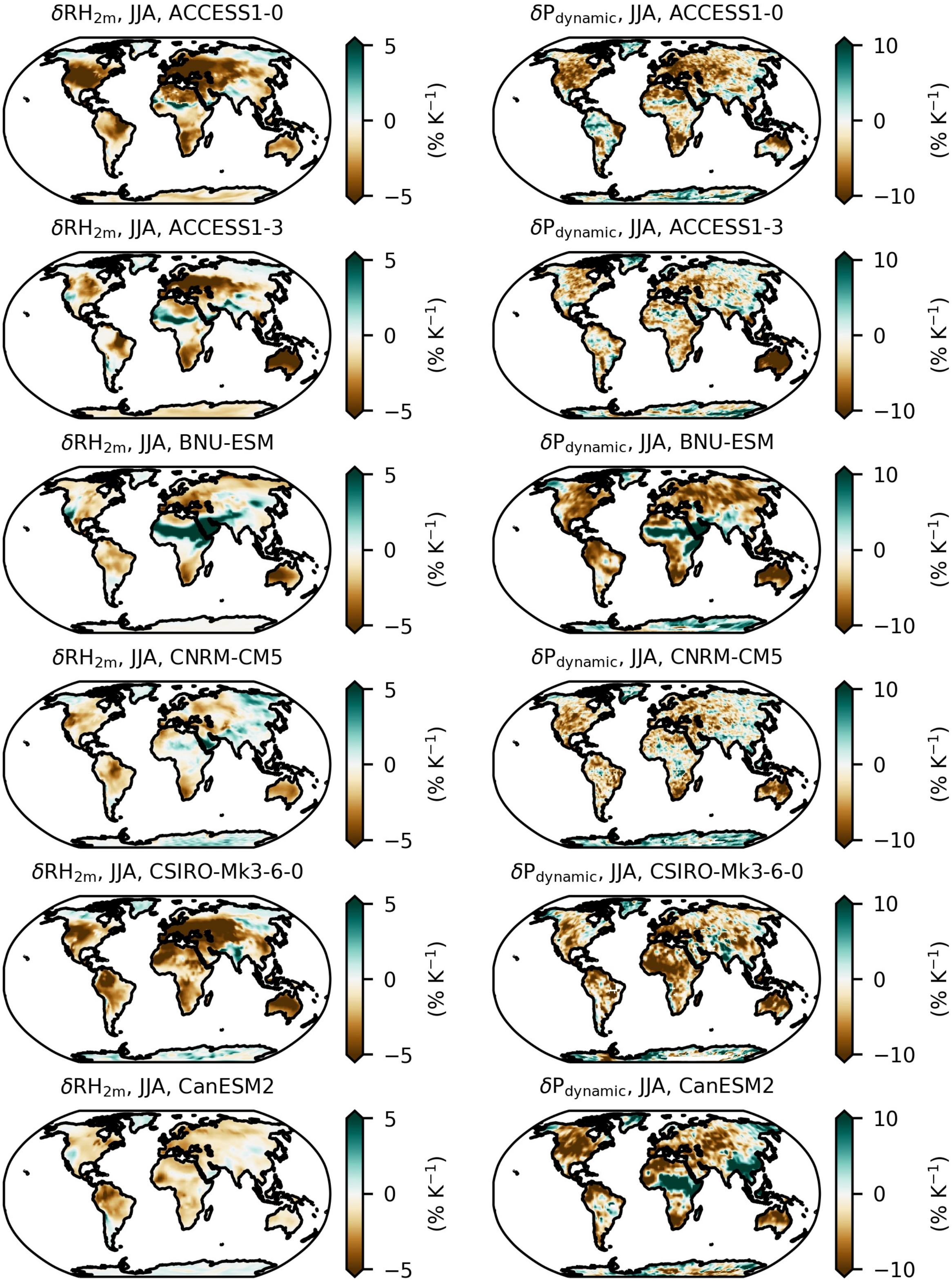

Figure S9. As in Fig.3a,b except showing the first six CMIP5 models individually.

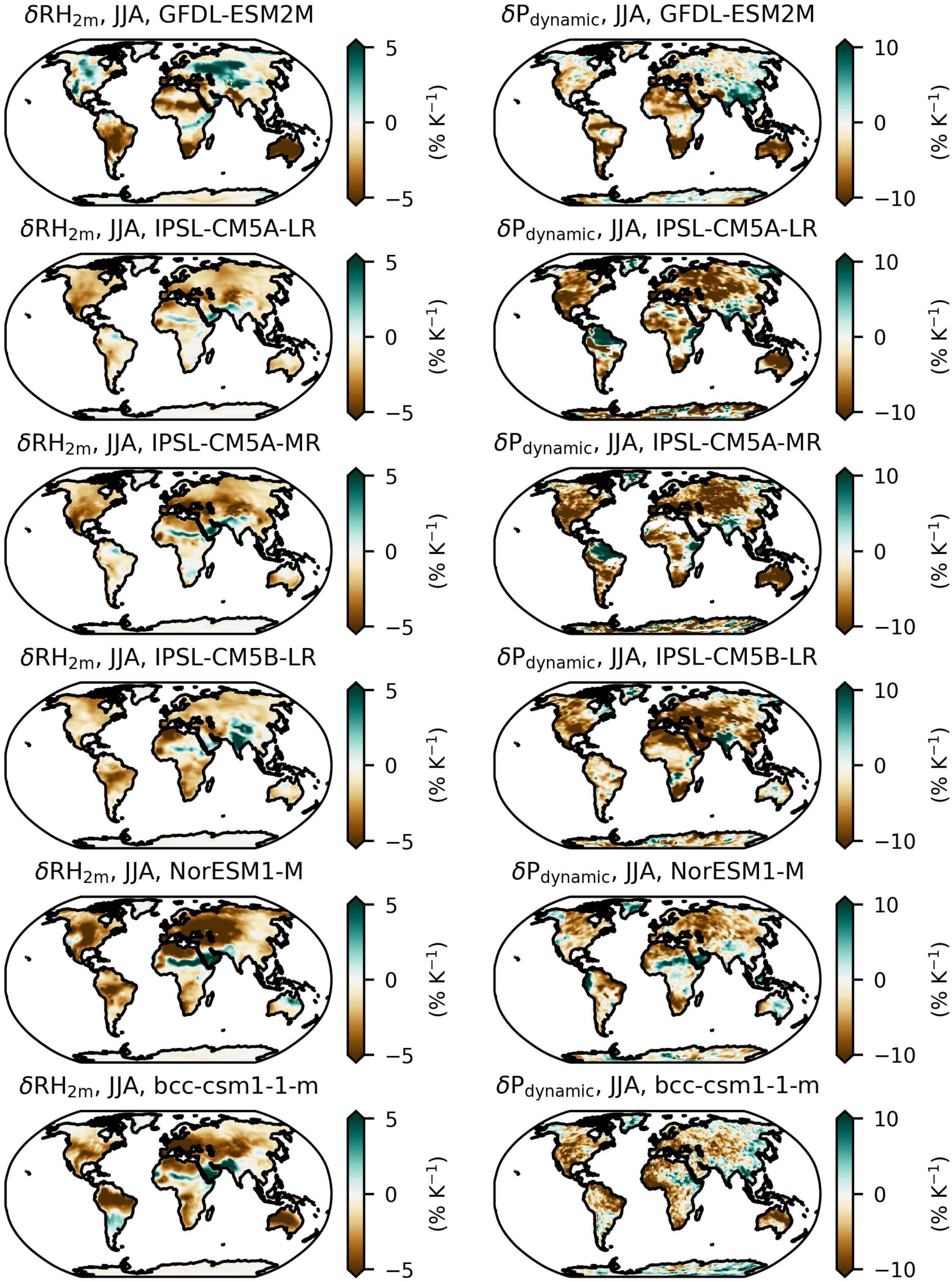

Figure S10. As in Fig.3a,b except showing the last six CMIP5 models individually.

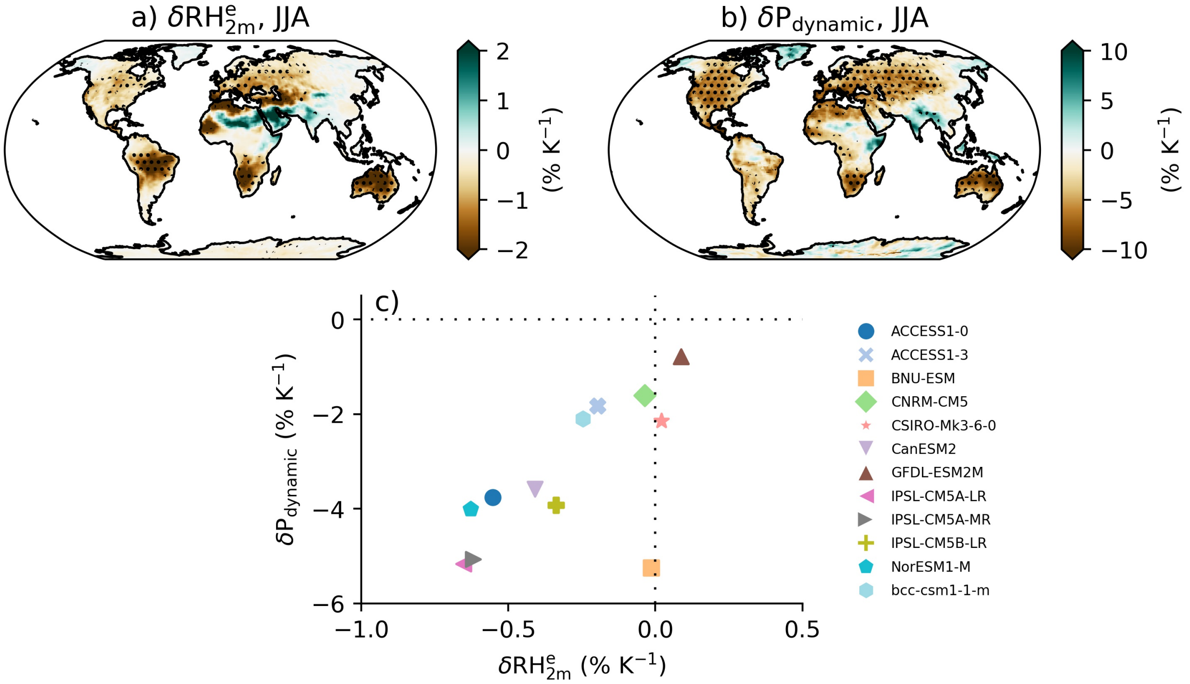

Figure S11. As in Fig. 3 of the main text, except we use RH_{2m} on the day of the extreme event in JJA (denoted using a superscript ^{e}), as opposed to the seasonal-mean RH_{2m}. The correlation in panel c is improved when we make this change, except for one outlier. However, RH^e_{2m} captures less of the spatial pattern and pattern of model agreement than seasonal-mean RH_{2m} over NH land.

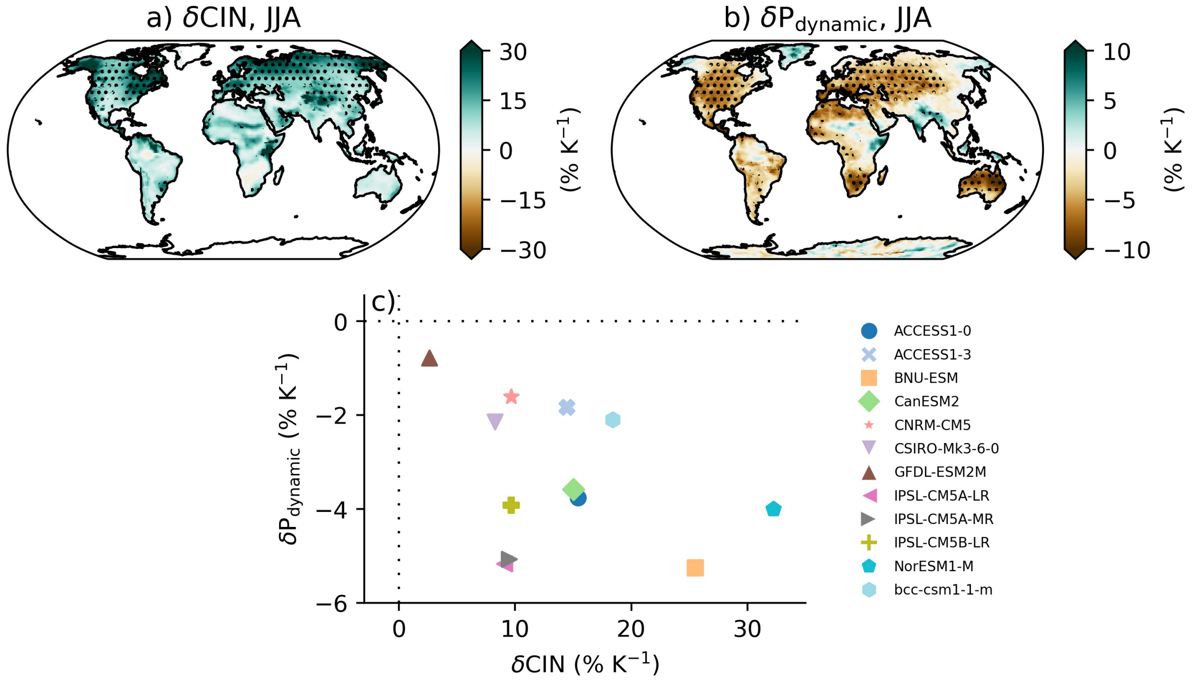

Figure S12. As in Fig. 3 of the main text, except we have replaced seasonal-mean RH_{2m} with seasonal-mean CIN. Seasonal-mean changes in CIN during JJA capture much of the spatial pattern of the dynamic contribution over NH land, and they also capture much of the inter-model spread in the dynamic contribution.

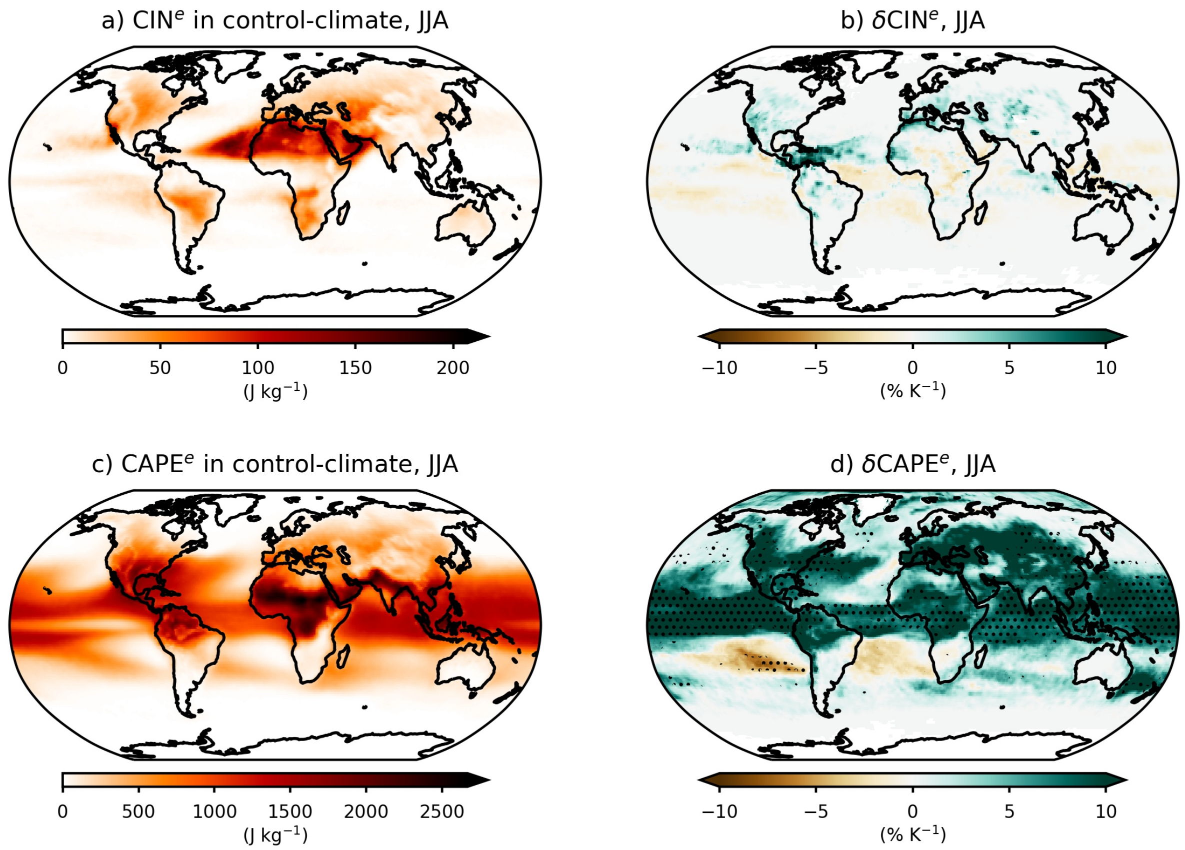

Figure S13. (a,c) Multi-model mean CAPE and CIN calculated on the day of the extreme event in JJA (denoted using a superscript ^{e}) and then averaged from 1950-2100. (b,d) Sensitivities of CIN^e and CAPE^e to warming, where stippling indicates 90% of models agree on the sign of the change.

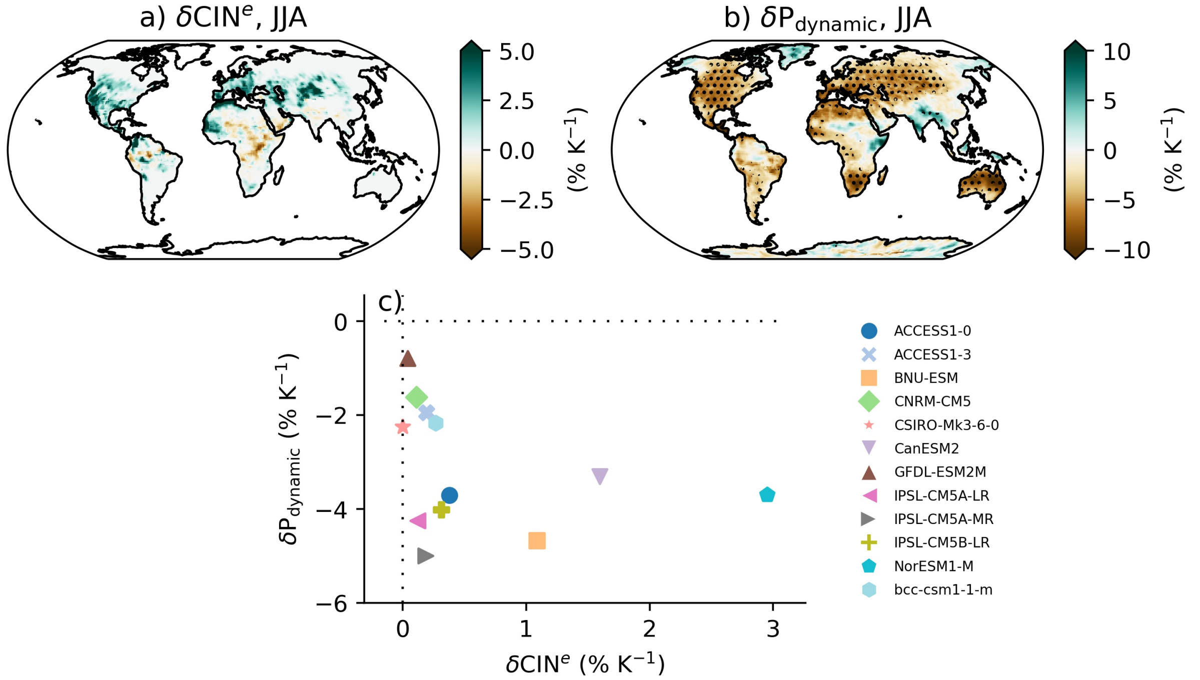

Figure S14. As in Fig. 3 of the main text, except we we have replaced seasonal-mean RH_{2m} with CIN calculated on the day of the extreme event in JJA (denoted using a superscript ^{e}). In panel (c) we calculate the scatter plot using the mean trends across 40-70°N land as opposed to using the median (as in previous figures). This is because most models exhibit negligible δCIN^e trends during JJA for greater than half of the grid-points over NH extratropical land, and so the median does not represent the inter-model scatter as faithfully as the mean.

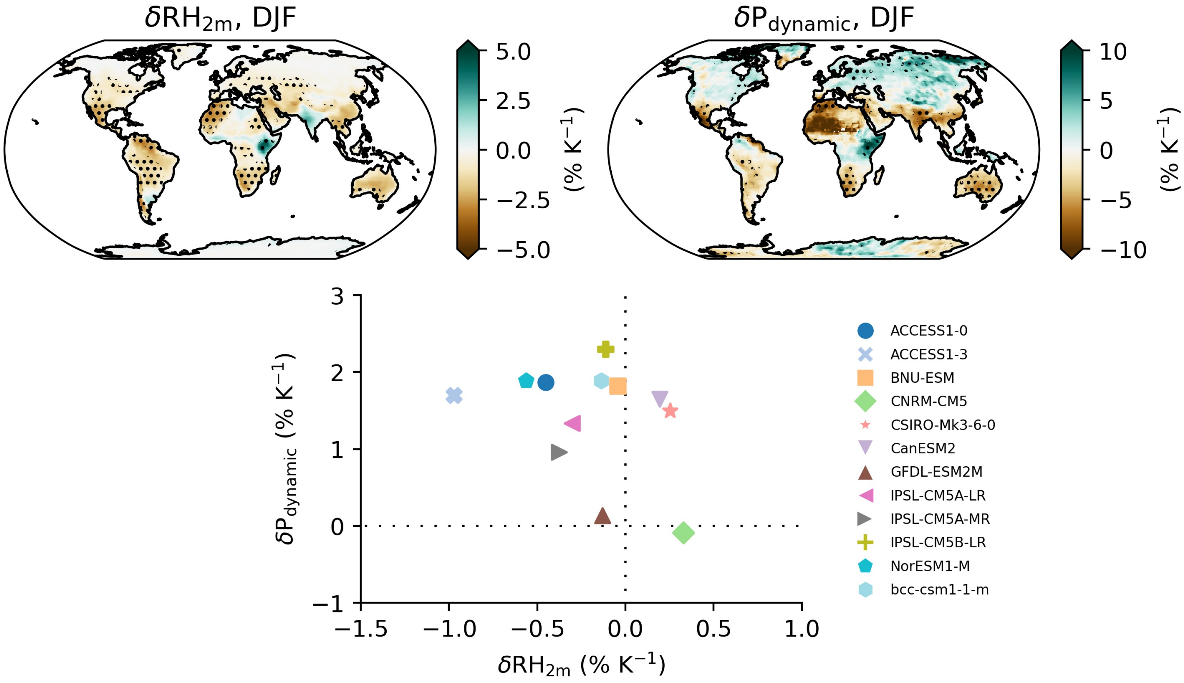

Figure S15. As in Fig. 3, but for DJF. Most models predict a weak decrease in near-surface relative humidity with warming over Northern Hemisphere land in DJF, but the dynamic contribution over Northern Hemisphere land is positive in this season. The lack of a correlation with near-surface relative humidity over the Northern Hemisphere during DJF is likely because precipitation extremes during DJF are associated with weather systems that are less strongly influenced by convection than during JJA.

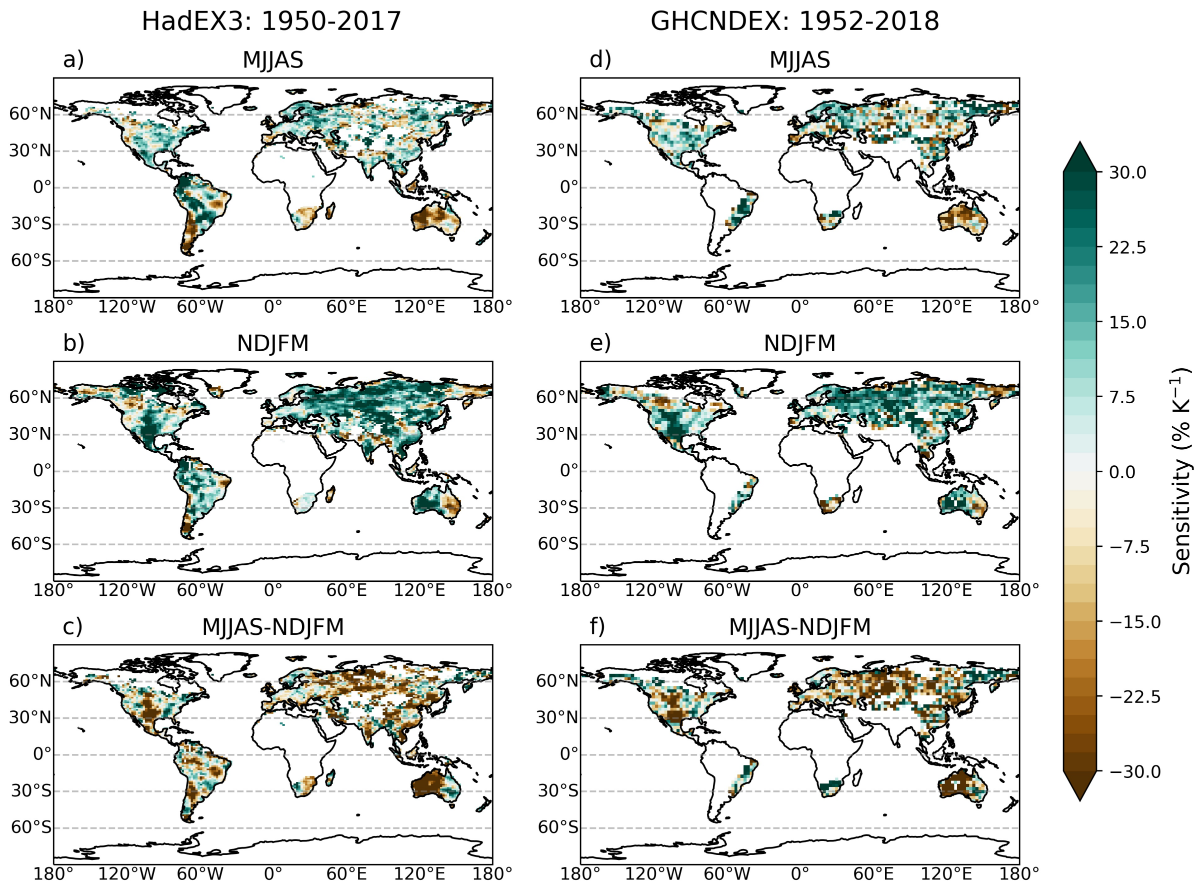

Figure S16. Regional sensitivities of Rx1day to global temperature changes over the period 1950-2017 for HadEX3 (a,b,c) and 1952-2018 for GHCNDEX (d,e,f). Sensitivities are plotted for (a,d) MJJAS and (b,e) NDJFM for grid boxes with at least 45 years of data, and (c,f) for the seasonal contrast, MJJAS-NDJFM, for grid boxes with at least 45 years with data for both MJJAS and NDJFM (see Section 2 of main text for details). The HadEX3 and GHCNDEX datasets have spatial resolutions of 1.25°x1.875° and 2.5°x2.5°, respectively. The figure shows that HadEX3 has substantially more grid boxes with data in the tropics. Visually it is also apparent that the extreme precipitation sensitivity is lower during MJJAS (a, d) than in NDJFM (b, d) in both datasets over the extratropical Northern Hemisphere, corresponding to a summer-winter contrast over this region (c, f).

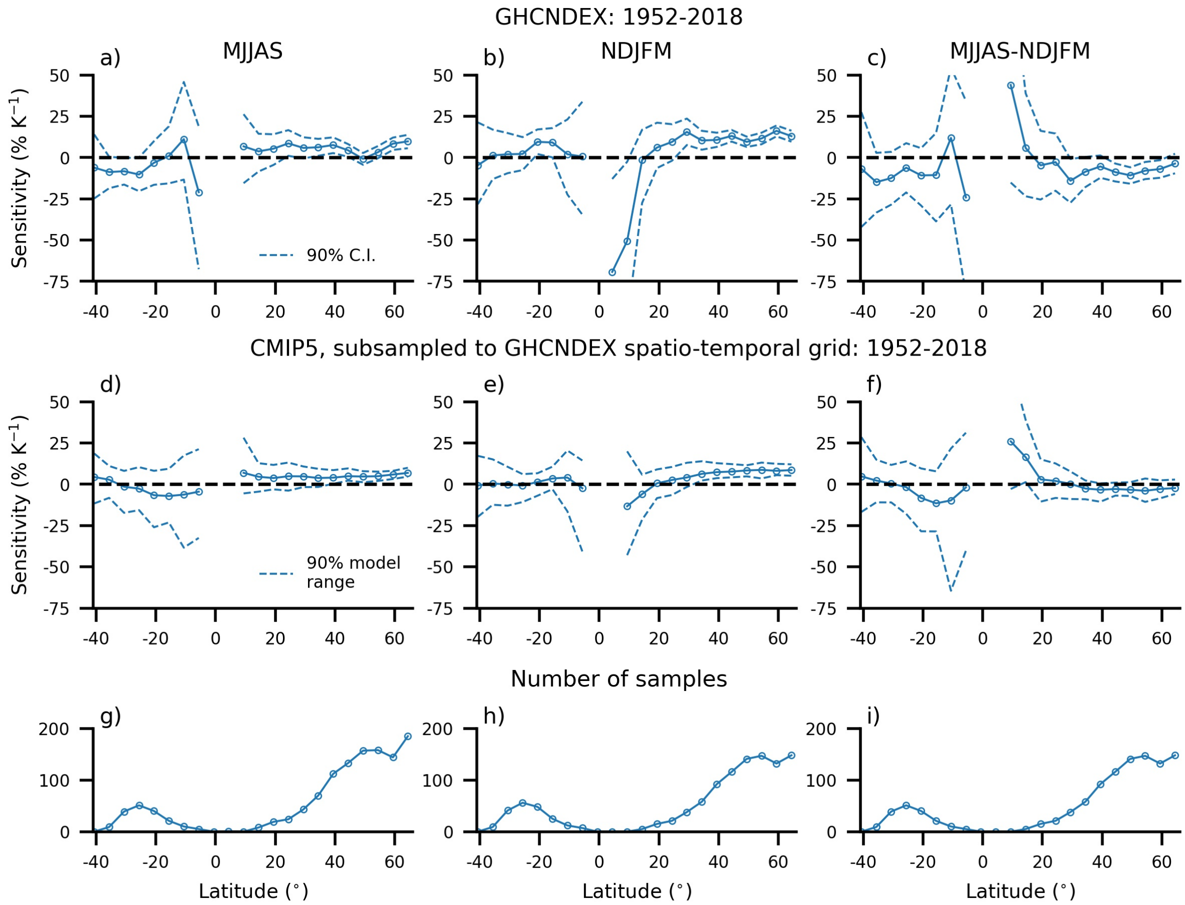

Figure S17. As in Fig. 4, except for the GHCNDEX observational dataset rather than HadEX3. CMIP5 simulations are subsampled to GHCNDEX in making this figure.

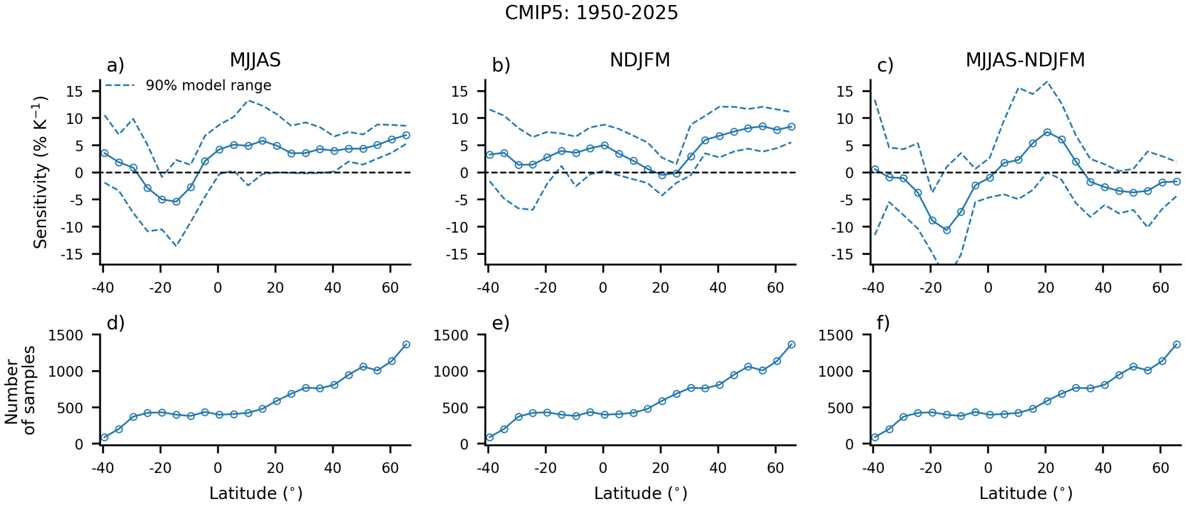

Figure S18. Sensitivity of seasonal Rx1day over land to warming in CMIP5 over the period 1950-2025 for (a) MJJAS, (b) NDJFM and (c) MJJAS-NDJFM. The sensitivities are calculated the same way as in Fig. 4 and Fig. S17 except for here we do not subsample the CMIP5 models to the spatio-temporal grid of the observations. The results show that the summer-winter contrast is also present in CMIP5 models when there is no missing data. The number of included gridboxes (d,e,f) is the same in each season, but there are latitudinal variations which reflect the fact there is less land in some 5° latitude bands than in others.